



# In situ vertical profiles of aerosol extinction, mass, and composition over the southeast United States during SENEX and SEAC<sup>4</sup>RS: observations of a modest aerosol enhancement aloft

N. L. Wagner<sup>1,2</sup>, C. A. Brock<sup>1</sup>, W. M. Angevine<sup>1,2</sup>, A. Beyersdorf<sup>3</sup>, P. Campuzano-Jost<sup>2,4</sup>, D. Day<sup>2,4</sup>, J. A. de Gouw<sup>1,2</sup>, G. S. Diskin<sup>3</sup>, T. D. Gordon<sup>1,2</sup>, M. G. Graus<sup>1,2,a</sup>, J. S. Holloway<sup>1,2</sup>, G. Huey<sup>5</sup>, J. L. Jimenez<sup>2,4</sup>, D. A. Lack<sup>1,2</sup>, J. Liao<sup>1,2</sup>, X. Liu<sup>5</sup>, M. Z. Markovic<sup>1,2,b</sup>, A. M. Middlebrook<sup>1</sup>, T. Mikoviny<sup>6</sup>, J. Peischl<sup>1,2</sup>, A. E. Perring<sup>1,2</sup>, M. S. Richardson<sup>1,2</sup>, T. B. Ryerson<sup>1</sup>, J. P. Schwarz<sup>1,2</sup>, C. Warneke<sup>1,2</sup>, A. Welti<sup>1,2,7</sup>, A. Wisthaler<sup>8</sup>, L. D. Ziemba<sup>3</sup>, and D. M. Murphy<sup>1</sup>

<sup>1</sup>NOAA Earth System Research Laboratory, 325 Broadway, Boulder, CO 80305, USA

<sup>2</sup>Cooperative Institute for Research in Environmental Sciences, University of Colorado, Boulder, CO 80309, USA

<sup>3</sup>NASA Langley Research Center, MS 483, Hampton, VA 23681, USA

<sup>4</sup>Department of Chemistry and Biochemistry, University of Colorado, Boulder, CO 80309, USA

<sup>5</sup>School of Earth & Atmospheric Sciences, Georgia Institute of Technology, Atlanta, GA 30332, USA

<sup>6</sup>Oak Ridge Associated Universities (ORAU), Oak Ridge, TN, USA

<sup>7</sup>Institute for Atmospheric & Climate Science, Swiss Federal Institute of Technology, Zürich, Switzerland

<sup>8</sup>Institute for Ion Physics and Applied Physics, University of Innsbruck, Technikerstrasse 25, 6020 Innsbruck, Austria

<sup>a</sup>now at: Institute of Meteorology and Geophysics, University of Innsbruck, Austria

<sup>b</sup>now at: Air Quality Research Division, Environment Canada, Toronto, ON, Canada

Correspondence to: N. L. Wagner (nick.wagner@noaa.gov)

Received: 30 December 2014 – Published in Atmos. Chem. Phys. Discuss.: 03 February 2015

Revised: 19 May 2015 – Accepted: 08 June 2015 – Published: 30 June 2015

**Abstract.** Vertical profiles of submicron aerosol from in situ aircraft-based measurements were used to construct aggregate profiles of chemical, microphysical, and optical properties. These vertical profiles were collected over the southeastern United States (SEUS) during the summer of 2013 as part of two separate field studies: the Southeast Nexus (SENEX) study and the Study of Emissions and Atmospheric Composition, Clouds, and Climate Coupling by Regional Surveys (SEAC<sup>4</sup>RS). Shallow cumulus convection was observed during many profiles. These conditions enhance vertical transport of trace gases and aerosol and create a cloudy transition layer on top of the sub-cloud mixed layer. The trace gas and aerosol concentrations in the transition layer were modeled as a mixture with contributions from the mixed layer below and the free troposphere above. The amount of vertical mixing, or entrainment of air from the free troposphere, was quantified using the observed mixing ratio of carbon monoxide (CO). Although the median aerosol mass, extinction, and volume decreased with altitude in the transition layer, they were ~10 % larger than expected from vertical mixing alone.

This enhancement was likely due to secondary aerosol formation in the transition layer. Although the transition layer enhancements of the particulate sulfate and organic aerosol (OA) were both similar in magnitude, only the enhancement of sulfate was statistically significant. The column integrated extinction, or aerosol optical depth (AOD), was calculated for each individual profile, and the transition layer enhancement of extinction typically contributed less than 10 % to the total AOD. Our measurements and analysis were motivated by two recent studies that have hypothesized an enhanced layer of secondary aerosol aloft to explain the summertime enhancement of AOD (2–3 times greater than winter) over the southeastern United States. The first study attributes the layer aloft to secondary organic aerosol (SOA) while the second study speculates that the layer aloft could be SOA or secondary particulate sulfate. In contrast to these hypotheses, the modest enhancement we observed in the transition layer was not dominated by OA and was not a large fraction of the summertime AOD.

## 1 Introduction

Shallow cumulus convection is common over the southeastern United States (SEUS) during the summer. It enhances the vertical transport of trace gases and aerosol and creates a transition layer between the mixed layer and free troposphere (Siebesma, 1998). Due to the presence of clouds and entrainment in the transition layer, it has also been referred to as the cloud layer and the entrainment zone. The transition layer is intermittently mixed by thermal plumes that originate in the mixed layer and form cumulus clouds that release latent heat within the layer. There have been several observations of vertical transport and redistribution of trace gases by shallow cumulus convection (Angevine, 2005; Ching and Alkezweeny, 1986; Ching et al., 1988; Greenhut, 1986), and a few studies have investigated the vertical transport and aerosol formation during cumulus convection (Ching et al., 1988; Sorooshian et al., 2006, 2007; Wonaschuetz et al., 2012).

Based on the seasonality of the surface-aerosol–aerosol-optical-depth (AOD) relationship in the SEUS and the spatial similarity of biogenic emissions and enhanced AOD, Goldstein et al. (2009) and Ford and Heald (2013) have hypothesized the existence of a layer of enhanced secondary aerosol aloft in the summer which contributes to AOD but not to surface measurements of aerosol mass. Goldstein et al. (2009) hypothesize that the aerosol layer is primarily secondary organic aerosol (SOA), while Ford and Heald speculate that the layer aloft could be either SOA or particulate sulfate. Although neither study speculates about meteorological mechanisms that would lead to the formation of this layer, aerosol production in the transition layer of shallow cumulus convection is a plausible mechanism that could produce the hypothesized layer. More generally, the vertical distribution of aerosol and aerosol formation are integral to understanding the relationship between aerosol mass ( $PM_{2.5}$ ) at the surface and AOD (Hoff and Christopher, 2009).

Submicrometer aerosol particles, which dominate aerosol mass, are largely secondary and composed of organic aerosol (OA) and sulfates during the summer in the SEUS (Edgerton et al., 2005; Weber et al., 2007). While the formation mechanisms of secondary particulate sulfate are well understood (e.g., Seinfeld and Pandis, 1998), the formation of SOA is more complex and uncertain. Both biogenic and anthropogenic precursor emissions are thought to be important (de Gouw and Jimenez, 2009). The relative importance of the homogenous and aqueous oxidation pathways for both sulfate and OA is also uncertain (Carlton and Turpin, 2013; Carlton et al., 2008; Eatough et al., 1994; Ervens et al., 2011; Luria and Sievering, 1991; McKeen et al., 2007). Based on the abundance of aerosol water and cumulus convection, aqueous processing is expected to be an important aerosol formation pathway in the SEUS (He et al., 2013), and processing in cloud droplets would occur primarily in the transition layer.

In this analysis, aircraft-based in situ measurements of aerosol chemical, physical, and optical properties are used

to examine the vertical structure of aerosol in the SEUS during shallow cumulus convection and to quantify aerosol enhancements in the transition layer and its contribution to summertime AOD. We use measurements made aboard the National Oceanic and Atmospheric Administration (NOAA) WP-3D aircraft during the Southeast Nexus (SENEX) study in June and July of 2013 and the National Aeronautic and Space Administration (NASA) DC-8 aircraft during SEAC<sup>4</sup>RS in August and September of 2013 to construct aggregate vertical profiles of aerosol extinction, mass, and composition as a function of altitude over the SEUS. The transition layer aerosol and trace gas concentrations are modeled as a mixture with contributions from the free troposphere and mixed layer. The in situ measurements of the extinction coefficient are used to calculate the AOD and contributions to the AOD from aerosol water, from the mixed layer, and from the transition layer.

## 2 Methods and measurements

In this analysis we combine data collected during two aircraft field studies that were partially conducted over the SEUS in the spring and summer of 2013. Although the SENEX study collected measurements in late spring and early summer while SEAC<sup>4</sup>RS collected measurements in the late summer, both studies encountered shallow cumulus convection. Additionally, both aircraft hosted a similar set of in situ instruments, which was conducive to a combined analysis.

### 2.1 SENEX

The SENEX study was part of the larger Southeast Atmosphere Study in the SEUS during June and July of 2013. The NOAA WP-3D aircraft flew 18 research flights based out of Smyrna, Tennessee, during June and July 2013 for SENEX with a payload of instruments measuring atmospheric trace gases, aerosol properties, and meteorological parameters. This analysis uses measurements of carbon monoxide (CO), carbon dioxide (CO<sub>2</sub>), methane (CH<sub>4</sub>), sulfur dioxide (SO<sub>2</sub>), isoprene, aerosol composition, and aerosol optical properties (Table 1). The aerosol was sampled downstream of a low turbulence inlet (Wilson et al., 2004) and an impactor with a 1  $\mu$ m aerodynamic diameter size cut. Before impaction, the sampled aerosol was initially dried by ram heating when sampling into the aircraft. The sampled aerosol was then dried further in each instrument.

The non-refractory aerosol composition was measured by a compact time-of-flight aerosol mass spectrometer (AMS) downstream of a pressure controlled inlet (Bahreini et al., 2008) and most (97 %) of the submicron volume measured by the aerosol sizing instruments was transmitted into the AMS during SENEX. The collection efficiency for the AMS was determined by the composition for each data point using the algorithm described by Middlebrook et al. (2012). When

comparing the volume derived from composition (AMS plus black carbon mass) to the volume measured by the aerosol sizing instruments in the manner outlined by Bahreini et al. (2009), 87 % of the aerosol composition and sizing data from the entire SENEX study is within the combined uncertainties.

## 2.2 SEAC<sup>4</sup>RS

SEAC<sup>4</sup>RS consisted of measurements aboard three aircraft based in Houston, Texas, during August and September of 2013. In this analysis, we focus on in situ measurements from the NASA DC-8 aircraft, which conducted 19 research flights. The measurements that were collected onboard the DC-8 and used in this analysis are summarized in Table 2. Unlike the SENEX study, there was no continuous measurement of methane during SEAC<sup>4</sup>RS. The aerosol extinction and black carbon instruments flown on the DC-8 during SEAC<sup>4</sup>RS were the same instruments used onboard the NOAA WP-3D aircraft during SENEX. Measurements of aerosol extinction, volume, and black carbon mass sampled aerosol through a shrouded diffuser inlet described by McNaughton et al. (2007). The aerosol extinction was measured downstream of 1  $\mu\text{m}$  impactor.

The non-refractory aerosol composition was measured by a high resolution time-of-flight AMS similar to the compact time-of-flight AMS used during the SENEX study. The two instruments differed in the resolution of the mass spectrometer. The higher resolution AMS used during SEAC<sup>4</sup>RS was operated with a 1 s sample interval. This AMS was operated similar to Dunlea et al. (2009) and also used a pressure-controlled inlet (Bahreini et al., 2008). The composition-dependent formulation of Middlebrook et al. (2012) was used to estimate the collection efficiency. The AMS sampled aerosol downstream of a HIMIL inlet (<http://www.eol.ucar.edu/homes/dcrogers/Instruments/Inlets/>). In both the HIMIL inlet and the shrouded diffuser inlet, the sampled aerosol was initially dried by ram heating and then further dried in each instrument.

## 2.3 Surface measurements

The Southeastern Aerosol Research and Characterization (SEARCH) Network consists of eight continuous monitoring ground sites in Georgia and Alabama hosting several gas-phase and aerosol measurements (Edgerton et al., 2005, 2006; Hansen et al., 2003). During SENEX the NOAA WP-3D flew over four of these sites a total of 15 times, and extinction near the surface is calculated using measurements of aerosol scattering (Radiance Research Model M903 nephelometer, Tempe, Arizona, USA) and absorption (Magee Scientific Model AE-16 Aethalometer, Berkeley, California, USA) at each SEARCH site to compare with the extinction measured onboard the NOAA WP-3D aircraft in the mixed layer.

## 2.4 Aerosol water

The enhancement of extinction due to condensation of water onto the aerosol is modeled using an empirical parameterization (shown in Eq. 1), hereafter referred to as the kappa parameterization (Brock et al., 2015). The hygroscopic growth of particle diameter is described by kappa-Koehler theory (Petters and Kreidenweis, 2007). A particle size distribution and a Mie scattering calculation would be necessary to rigorously extend the kappa-Koehler theory to the hygroscopic enhancement of optical properties. However, Brock et al. (2015) shows that when atmospheric accumulation mode size distributions typical of the SEUS are used, the functional form of kappa-Koehler theory can be applied directly to the optical extinction (Eq. 1).

$$\sigma_{\text{ext}}(\text{RH}) = \sigma_{\text{ext}}(\text{dry}) \times \left( 1 + \kappa_{\text{opt}} \times \left( \frac{\text{RH}}{100 - \text{RH}} \right) \right). \quad (1)$$

The humidified extinction coefficient  $\sigma_{\text{ext}}(\text{RH})$  is a function of the dry extinction  $\sigma_{\text{ext}}(\text{dry})$  and the hygroscopicity parameter  $\kappa_{\text{opt}}$ . We note that  $\kappa_{\text{opt}}$  is based on the measurement of humidified extinction rather than the direct measurement of the diameter growth factor or activation fraction, i.e., humidified tandem differential mobility analyzers and cloud condensation nuclei counters. The aerosol extinction is measured in three separate constant RH channels: in dry conditions (RH less than 30 %), medium (RH typically 70 %), and high (RH greater than 80 %). The hygroscopicity parameter ( $\kappa_{\text{opt}}$ ) is determined by fitting the three measurements of extinction to Eq. (1). The resulting  $\kappa_{\text{opt}}$  and  $\sigma_{\text{ext}}(\text{dry})$  are then used to estimate the extinction at ambient RH. Lower values of aerosol hygroscopicity generally correspond to mineral dust, aerosol with high soot fraction, or primary OA such as fresh biomass burning emissions or automotive emissions (Masoni et al., 2009; Quinn et al., 2005). High hygroscopicity usually corresponds to an oxidized, aged aerosol, large sulfate mass fractions, and/or sea salt aerosol.

The calculated ambient extinction will differ from the actual ambient extinction in three cases. First, if the hygroscopic growth exhibits hysteresis and the ambient RH is below the deliquesce RH, ambient particles may be on the deliquescing (lower) or efflorescing (upper) branch of the hysteresis curve (Santarpia et al., 2004). Our extinction measurements cannot distinguish between these two states, because the sample aerosol is first dried. Then the aerosol is humidified to RH greater than 90 % in a cooled Nafion humidifier. The temperature of the humidifier (10–15 K below instrument temperature for 70 % RH and 1–3 K below for 90 % RH) is varied to control amount of water vapor added to the sample and maintain a constant RH in the sample cell. Finally the sample aerosol is reheated to the instrument temperature and measured in the sample cell. (The sample aerosol is exposed to elevated RH for a duration of 4 s before measurement.) Hence, the measured extinction at high RH and the subsequently calculated hygroscopicity param-

**Table 1.** Measurements aboard the NOAA WP-3D used in this analysis. The sample interval corresponds to the rate at which data are reported and is the integration time for the lower limit of detection.

Measurement	Technique	Sample interval	Lower limit of detection	Accuracy	Reference
Dry sub-micrometer aerosol extinction (532 nm)	Cavity ring-down spectrometer	1 s	0.1 Mm <sup>-1</sup>	5 % (RH < 30 %)	Langridge et al. (2011)
Humidified sub-micrometer aerosol extinction (532 nm)	Cavity ring-down spectrometer	1 s	0.1 Mm <sup>-1</sup>	11 % (RH = 90 %)	Langridge et al. (2011)
Sub-micrometer aerosol composition	Compact time-of-flight aerosol mass spectrometer	10 s	OA < 0.4 μg m <sup>-3</sup> SO <sub>4</sub> < 0.05 μg m <sup>-3</sup>	38 % OA 34 % Inorg.	Drewnick et al. (2005); Canagaratna et al. (2007)
Sub-micrometer aerosol volume	Optical particle counter	1 s	0.03 μm <sup>3</sup> cm <sup>-3</sup>	+26 %, -12 %	Cai et al. (2008)
CO	Vacuum ultraviolet fluorescence	1 s	0.5 ppbv	5 %	Holloway et al. (2000)
Isoprene	Proton transfer reaction mass spectrometer	14 s	< 32 pptv	20 %	de Gouw and Warneke (2007)
Dew point (RH)	Chilled mirror hygrometer	1 s	–	0.2 °C	–
Black carbon mass	Single particle soot photometer	1 s	12 ng m <sup>-3</sup>	30 %	Schwarz et al. (2008)
SO <sub>2</sub>	Pulsed ultraviolet fluorescence	1 s	250 pptv	20 %	Ryerson et al. (1998)
CH <sub>4</sub>	Cavity ring-down spectrometer	1 s	–	1.2 ppbv	Peischl et al. (2012)
CO <sub>2</sub>	Cavity ring-down spectrometer	1 s	–	0.15 ppmv	Peischl et al. (2012)

**Table 2.** Measurements aboard the NASA DC-8 used in this analysis. The sample interval corresponds to the rate at which data are reported and is the integration time for the lower limit of detection.

Measurement	Technique	Sample interval	Lower limit of detection	Accuracy	Reference
Dry sub-micrometer aerosol extinction (532 nm)	Cavity ring-down spectrometer	1 s	0.1 Mm <sup>-1</sup>	5 % (RH < 30 %)	Langridge et al. (2011)
Humidified sub-micrometer aerosol extinction (532 nm)	Cavity ring-down spectrometer	1 s	0.1 Mm <sup>-1</sup>	11 % (RH = 90 %)	Langridge et al. (2011)
Sub-micrometer aerosol composition	High resolution time-of-flight aerosol mass spectrometer	1 s	0.6 μg m <sup>-3</sup> OA 0.06 μg m <sup>-3</sup> SO <sub>4</sub> 0.06 μg m <sup>-3</sup> NO <sub>3</sub> 0.01 μg m <sup>-3</sup> NH <sub>4</sub>	38 % OA 34 % Inorg.	Canagaratna et al. (2007)
Sub-micrometer aerosol volume	Optical particle counter	1 s	0.03 μm <sup>3</sup> cm <sup>-3</sup>	+26, -12 %	Cai et al. (2008)
CO	Infrared absorption	1 s	0.5 ppbv	5 %	Sachse et al. (1987)
Isoprene	Proton transfer reaction mass spectrometer	14 s	25 pptv	10 %	de Gouw and Warneke (2007)
Dew point (RH)	Chilled mirror hygrometer	1 s	–	0.2 °C	–
Black carbon mass	Single particle soot photometer	1 s	12 ng m <sup>-3</sup>	30 %	Schwarz et al. (2008)
SO <sub>2</sub>	Chemical ionization mass spectrometer	1 s	9 pptv	15 %	Kim et al. (2007)
CO <sub>2</sub>	Infrared absorption	1 s	–	0.2 ppm	Vay et al. (2011)

ter  $\kappa_{\text{opt}}$  represent the hygroscopic growth of an efflorescing aerosol on the upper branch. If the aerosol undergoes hysteresis, we expected most aerosol in the summertime SEUS to be on the upper branch because the aerosol regularly pass through clouds and are exposed to high RH conditions. The aerosol also rarely experiences dry conditions (RH less than 30 %). Second, because the kappa parameterization produces an ambient extinction that asymptotically approaches infinity as RH approaches 100 %, we used ambient RH to calculate the ambient extinction only when RH was less than 95 % and assumed a constant RH of 95 % when ambient RH is greater than or equal to 95 %. Therefore, the calculated ambient extinction is a lower limit of the ambient extinction when RH was greater than 95 %. Third, in the case that supermicrometer particles (which are not sampled by instruments used in this analysis) make a significant contribution, the ambient extinction is underestimated. This is typically the case

during dust events and during in-cloud sampling, which were either not observed or excluded from this analysis, respectively.

## 2.5 Aggregation of vertical profiles

Individual profiles are affected by horizontal advection which couples spatially inhomogeneous emissions to the vertical profiles. Because of vertical wind shear and spatial variability during slant profiles, the vertical layers in an individual profile are not always directly comparable. The aggregation of the individual profiles is used to reduce the influence of this variability and resolve the typical vertical structure and mixing over the SEUS. Individual vertical profiles were selected from the research flights by inspection of the altitude time series and are generally included for all ascents and descents with an altitude difference greater than 1 km. Measurements during level flight legs were not used in this analysis.

Although cloud penetration was mostly avoided, aerosol data sampled during cloud penetration events were excluded due to the effects of particle shattering in the inlets. Cloud penetration events were identified using the video from the nose of the aircraft and cloud particle imaging probes mounted near the wing tips. Transects of biomass burning plumes were identified using tracers such as the acetonitrile mixing ratio, were typically during level flight legs, and were not found during any of the profiles used in this analysis. Extensive aerosol parameters (mass, extinction, volume) have been corrected to standard temperature (273.15 K) and pressure (1013 hPa). All calculated quantities such as ambient extinction and transition layer enhancements were determined before aggregation and then were aggregated in the same manner as the observations.

For the SENEX campaign, the vertical profiles (which were located primarily over northern Georgia and Alabama) were generally included in the flight plans for three purposes: to characterize the background boundary layer structure before and after urban and power plant plume intercepts, to characterize the vertical structure over surface measurement sites, and as enroute ascents and descents into and out of the region of interest. The SEAC<sup>4</sup>RS profiles that we use were distributed through Mississippi and Alabama and were conducted to characterize inflow and outflow near convective systems, to examine boundary layer chemistry over the SEUS, and as enroute ascents and descents. The individual vertical profiles used here include both spiral and slant ascents and descents and were typically between 5 and 15 min in duration.

In this analysis we construct two types of aggregate profiles. The first includes all of the afternoon vertical profiles over the SEUS and is binned according to altitude above ground level (“altitude-binned” aggregate profiles). The second type of aggregate includes only the subset of profiles during which shallow cumulus convection was present and is binned according to a normalized altitude described in Sect. 3.2 (“normalized” aggregate profiles). The profiles not included in the normalized aggregates were either collected during deeper convection and/or had a more complicated structure.

For the altitude-binned profiles, we have chosen all of the available vertical profiles from both SENEX and SEAC<sup>4</sup>RS over Mississippi, Alabama, and Georgia in the afternoon between 12:00 p.m. and 6:30 p.m. central daylight time, when we expect the boundary layer structure to be well developed and without residual layers left over from the previous day. The aggregate includes 74 profiles of which 41 profiles are from 6 research flights during SENEX and 33 profiles from 6 research flights during SEAC<sup>4</sup>RS. The locations of the profiles used in the altitude-binned aggregate are shown in Fig. 1. The data from individual vertical profiles were aggregated into 150 m vertical bins from the surface to 4.5 km based on the altitude above ground level. The vertical bin height of 150 m was chosen such that the slower measure-

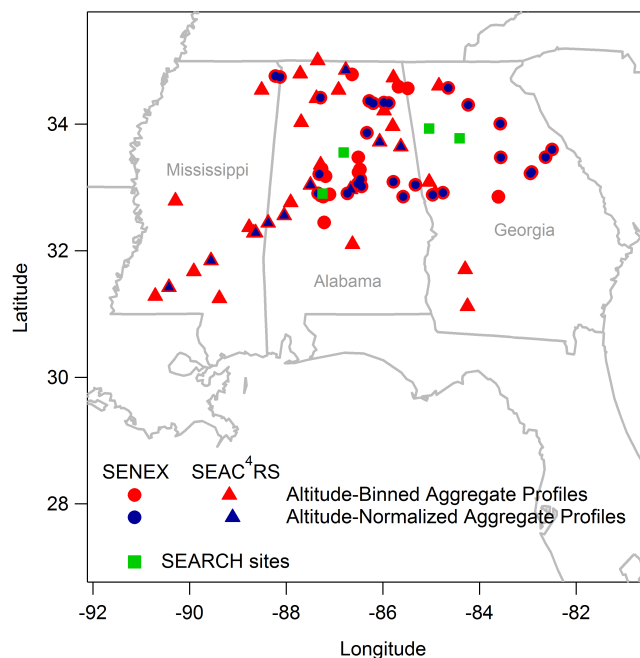


**Figure 1.** The locations of the vertical profiles from the SENEX (circles) and SEAC<sup>4</sup>RS (triangles) and SEARCH monitoring sites (green squares). The markers (both red and blue) are the locations of afternoon profiles used to construct the altitude-binned aggregate profile that includes 74 profiles: 41 from SENEX and 33 from SEAC<sup>4</sup>RS. The blue markers show the location of the profiles used to construct the altitude-normalized aggregate profile that includes 37 profiles: 27 from SENEX and 10 from SEAC<sup>4</sup>RS.

ments (aerosol mass and isoprene) typically contributed at least one datum to each bin for each individual profile. In each bin with data from five or more individual profiles, the median, interquartile range (IQR), and interdecile range were calculated. The median and percentiles were used because these statistics are more robust when outliers are present. The number of vertical profiles which contribute to each aggregated altitude bin varies with altitude because of the differences of the starting and ending altitudes of each individual profile (Fig. 2a). During some profiles or some portions of a profile, individual measurements of trace gases and aerosol properties did not report data (e.g., due to zeroing or calibrations).

The normalized aggregate profiles were calculated using only those individual profiles obtained during shallow cumulus convection and were altitude-normalized as described below. Shallow cumulus convection is common over the SEUS. Warren et al. (2007) have compiled a global cloud climatology based on surface observations. According to their work, the mean frequency of daytime cumulus clouds is 49 % over Alabama during June, July, and August, and the mean cloud coverage when cumulus clouds are present is 35 %. The presence of shallow cumulus convection during individual profiles was determined by inspection of visible images from

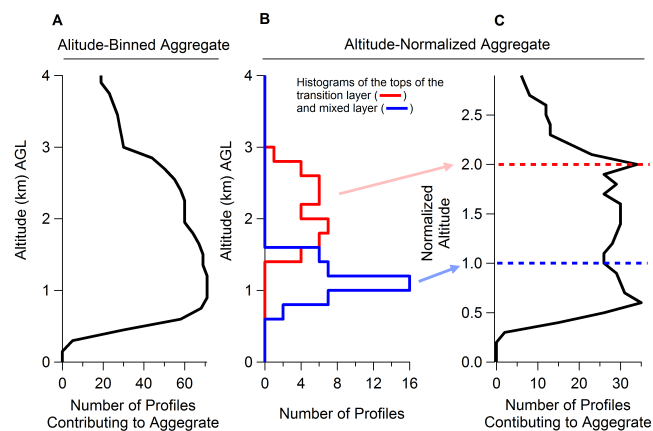


**Figure 2.** (a) The number of profiles that contribute to the altitude-binned aggregate, (b) histograms of the altitude of the tops of the transition and mixed layers, and (c) the number of profiles that contribute to the altitude-normalized aggregate.

the GOES satellite and the presence of a three layer structure (mixed layer, transition layer, and free troposphere), which is expected during shallow cumulus convection. The second aggregate includes 37 of the 74 SEUS profiles from the first aggregate. The locations of profiles in the second aggregate are shown in Fig. 1, and Fig. 2b shows the distributions of the mixed layer and transition layer heights determined from individual profiles which had medians of 1.2 and 2.2 km, respectively. For cumulus convection the height of the planetary boundary layer is defined as the cloud base or the top of the mixed layer; however, we find the term planetary boundary layer confusing in the context of shallow cumulus convection and have avoided using it. Determination of the mixed layer height and transition layer height is described in Sect. 3.2. For the normalized aggregate profiles, there are 25 bins assigned to each layer. Figure 2c shows the number of profiles that contribute to the second aggregate at each normalized altitude. The number of profiles varies with normalized altitude due to variability in the starting and ending altitudes of each profile and because the second aggregate is limited to portions of the individual profiles when aerosol mass, extinction, volume, and CO measurements all report data. Limiting data as such facilitates quantitative comparison of the aggregate profiles. In contrast, the first aggregate is constructed using all available data.

### 3 Results

#### 3.1 Altitude-binned aggregate profile

Altitude-binned aggregate profiles of dry and ambient aerosol extinction show several characteristics of note (Fig. 3). The median 532 nm dry extinction coefficient (Fig. 3a) is approximately independent of altitude below 1.5 km with median value of  $50 \text{ Mm}^{-1}$ , and the interquar-

tile range is 27 to  $73 \text{ Mm}^{-1}$ . The interquartile (25–75th percentiles) and interdecile (10–90th percentiles) ranges are due largely to variation between individual profiles rather than intra-profile point-to-point variation. Above 1.5 km the extinction coefficient decreases with altitude to a median value of  $6 \text{ Mm}^{-1}$  above 3.0 km. The gradual decrease in extinction with altitude from 1.2 to 2.5 km is due to the variation of mixed layer and transition layer heights in the individual profiles. Figure 3b shows the RH increasing with increasing altitude below 1.2 km. Above this level the RH has a slight decreasing trend with altitude and a large interquartile range spanning 30–70%. The relative humidity of the aggregate profile could be biased low, because during SENEX the flight dates were chosen to avoid precipitation and cloud penetration was mostly avoided during flights. However, this was not the case during SEAC<sup>4</sup>RS.

The median hygroscopicity parameter ( $\kappa$ , Fig. 3c) increases from 0.11 at the bottom of the profile to 0.18 at 3 km and is more variable above 3 km. The hygroscopic growth of the aerosol enhances the ambient extinction (Fig. 3d) throughout the profile and significantly between 0.7 and 1.7 km. The ambient extinction coefficient increases with altitude below 1.2 km due to increasing RH and decreases with altitude above 1.2 km due to a combination of decreasing RH and decreasing dry extinction. The hygroscopic growth of aerosol and the subsequent enhancement of extinction aloft could explain some of the enhancement of AOD noted by Goldstein et al. (2009) and Ford and Heald (2013).

The minimum altitude of individual aircraft profiles ranged from 300 to 700 m above the surface. We estimate the profile of dry extinction between the surface and the minimum altitude of the profiles by combining aircraft measurements made in the mixed layer in the vicinity of surface monitoring sites using ground data from those sites. During the SENEX study, there were 15 overflights in the mixed layer within 10 km of four SEARCH monitoring sites. The surface aerosol extinction at each SEARCH site was calculated using the aerosol scattering coefficient measured by a nephelometer with a center wavelength of 530 nm and the aerosol absorption coefficients measured by an aethalometer at 880 nm. Because the optical absorption at this wavelength was likely due to black carbon aerosol, we corrected the absorption coefficient to 530 nm using an Ångström exponent of 1, which is conventionally used for black carbon (Bergstrom et al., 2002; Lack and Langridge, 2013). Absorption typically accounted for less than 5% of the extinction. The calculated 530 nm surface extinction was not corrected to the 532 nm aircraft extinction because the correction would be less than 1%. The surface and aircraft extinction coefficients are correlated ( $R^2 = 0.91$ ), and the slope of a orthogonal distance regression fit to the data indicates that the aircraft data are  $\sim 6\%$  lower than the surface measurements (Fig. 4), which is within the combined uncertainty in the measurements. We conclude that the dry extinction is roughly independent of altitude from the surface to the top of the well-mixed layer.

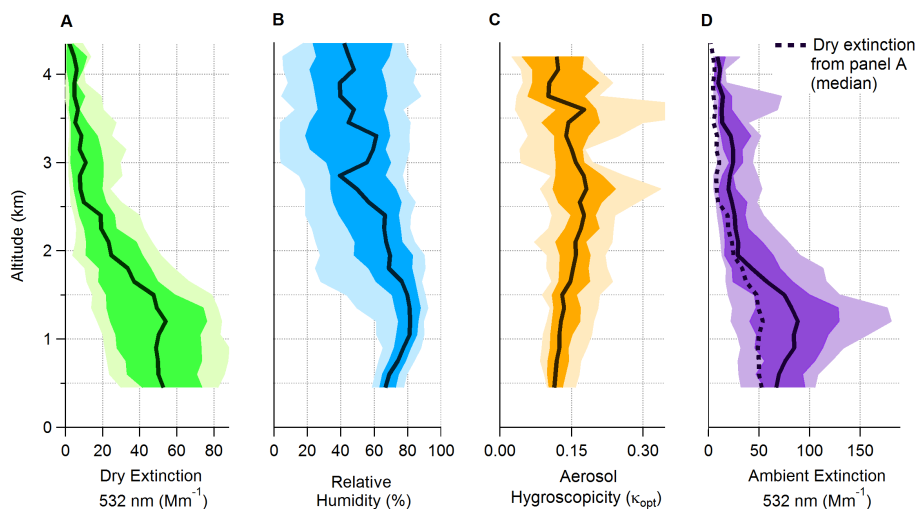


**Figure 3.** Altitude-binned aggregate profiles of (a) the 532 nm dry aerosol extinction, (b) relative humidity (calculated from dew point measurements), (c) aerosol hygroscopicity (humidified extinction measurements fit to Eq. 1), and (d) the calculated ambient extinction (Eq. 1). The shaded regions show the interdecile range (light) and the interquartile range (medium), and the solid lines are the median (dark). The dashed line in (d) shows the median dry extinction for comparison.

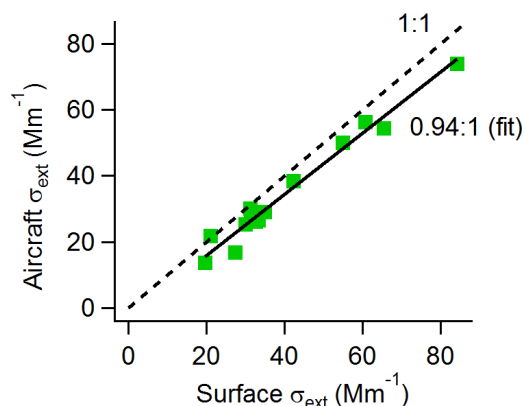


**Figure 4.** Comparison of airborne and surface measurements of the dry aerosol extinction coefficient. The airborne measurements are aboard the NOAA WP-3 aircraft. The surface measurements are from the SEARCH monitoring sites.

Crumeyrolle et al. (2014) found similar agreement between surface and aircraft-based boundary layer measurements of ozone in the Baltimore–Washington metropolitan area.

The altitude-binned aggregate vertical profile of aerosol mass (Fig. 5a) is similar in shape to the dry extinction profile. The median mass is  $13.7 \mu\text{g m}^{-3}$  at the bottom of the profile and decreases to  $2.1 \mu\text{g m}^{-3}$  above 3 km. The aerosol mass is the total of all ions measured by the AMS, and these ions are typically classified as  $\text{SO}_4$ ,  $\text{NH}_4$ ,  $\text{NO}_3$ , and OA. The inorganic ions are typically formed by ionization of simple salts such as ammonium sulfate and ammonium nitrate but may be formed from more complex compounds (i.e., organosulfates, organonitrates, and amines) that produce both inor-

ganic and organic ions when ionized. To indicate this complexity, we have omitted ionic charges from the notation (i.e.,  $\text{SO}_4$ ,  $\text{NH}_4$ ,  $\text{NO}_3$ ). In this classification scheme, the composition (Fig. 5b) of the submicron aerosol is primarily OA, sulfate, and ammonium. The mass fraction of the inorganic components ( $\text{NO}_3$ ,  $\text{NH}_4$ , and  $\text{SO}_4$ ) increases with altitude up to 3 km, while the OA mass fraction decreases with altitude up to 3 km. Above 3 km, the OA fraction increases; however, at this altitude the median aerosol mass is only  $2 \mu\text{g m}^{-3}$ . The increase of aerosol hygroscopicity with altitude up to 3 km corresponds with the increasing inorganic fraction of the aerosol. In particular, sulfate is typically more hygroscopic than OA and is 20 % of the aerosol mass at the bottom of the profile and 28 % of the aerosol mass at 3 km.

### 3.2 Normalized aggregate profiles

The heights of the mixed and transition layers varies among individual vertical profiles and this variation obscures the transition layer in the altitude-binned aggregate profile presented in Figs. 3 and 5. For example, the layer structure is clear in a semi-rural profile measured in the vicinity of shallow cumulus convection over central Georgia on the afternoon of 16 June (Fig. 6). The mixed layer is closest to the surface, a transition layer is formed above the mixed layer, and the free troposphere is on top.

The layered structure is evident in both the physical parameters such as virtual potential temperature ( $\Theta_v$ ) and ambient temperature as well as chemical mixing ratios such as carbon monoxide (CO) and isoprene. In the mixed layer, adiabatically conserved parameters such as virtual potential temperature (Fig. 6a) are independent of altitude. However, in the transition the virtual potential temperature increases with al-

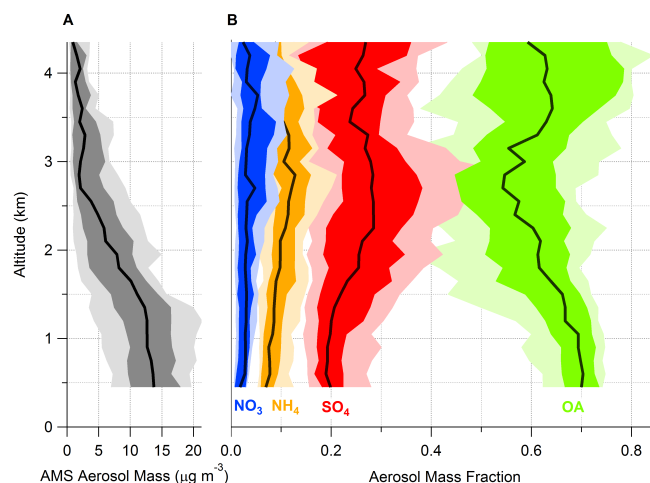


**Figure 5.** Aggregate profiles of (a) the aerosol mass and (b) the mass fractions of nitrate, ammonium, sulfate, and OA. The shaded regions show the interdecile range (light) and the interquartile range (medium), and the solid lines are the median (dark).

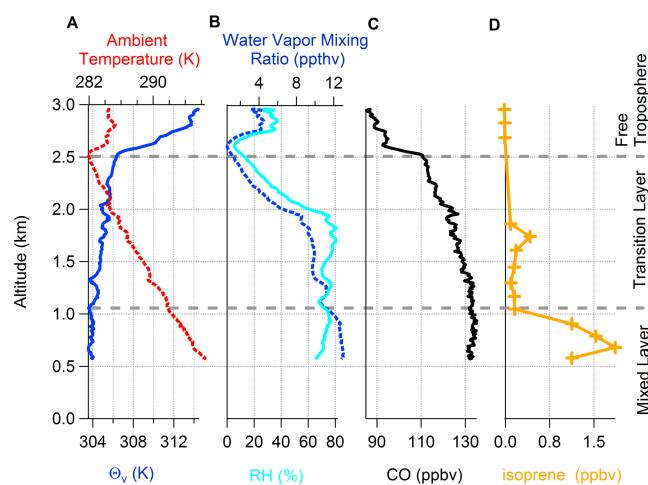


**Figure 6.** An example profile collected over central Georgia in the afternoon of 16 June showing (a) the temperature and virtual potential temperature, (b) the relative humidity and the water vapor mixing ratio, (c) the mixing ratio of CO that has a long lifetime, and (d) the mixing ratio of isoprene that has a short lifetime.

titude until the top of the transition layer is reached where a capping temperature inversion is present. In the mixed layer, the mixing ratio of water vapor is also independent of altitude; however, RH increases with altitude as temperature decreases (Fig. 6b). Relative humidity is high in the transition layer, and video from the nose of the aircraft confirms the presence of clouds in this layer.

The transition layer is also evident in the comparison of long-lived trace gases such as CO (Fig. 6c) with short lifetime trace gases such as isoprene (Fig. 6d). Carbon monoxide is directly emitted during combustion, produced by oxida-

tion of hydrocarbons, lost to oxidation by OH, and typically has an atmospheric lifetime of 1–4 months which varies seasonally and regionally (Seinfeld and Pandis, 1998). In this profile, the CO mixing ratio is greater than 110 ppbv in both the mixed and transition layers and decreases to less than 100 ppbv in the free troposphere. In the mixed layer the CO mixing ratio is independent of altitude and decreases modestly with altitude in the transition layer. Isoprene is a short-lived trace gas that typically has an atmospheric lifetime less than 2 h (Seinfeld and Pandis, 1998) and in the summertime is emitted by vegetation common in the SEUS. In the mixed layer, the isoprene mixing ratio is greater than 1 ppbv and variable due to heterogeneous surface emissions (Fig. 6d). The isoprene mixing ratio in the transition layer is always less than 500 ppbv and typically  $\sim 10\%$  of the mixed layer value. In the free troposphere, the isoprene mixing ratio is below the detection limit of the measurement.

To examine vertical structure in more detail, altitude-normalized aggregate profiles were calculated. Altitude normalization is commonly done by dividing the altitude by the height of the mixed layer. However, because of the more complex vertical structure often encountered during shallow cumulus convection, we have defined a normalized altitude,  $h_{\text{norm}}$ , for each profile such that the top of the mixed layer,  $h_{\text{ML}}$ , is assigned a normalized altitude of 1, and the top of the transition layer,  $h_{\text{TL}}$ , is assigned a normalized altitude of 2:

$$\begin{aligned} 0 < h < h_{\text{ML}} & \quad h_{\text{norm}} = h/h_{\text{ML}} \\ h_{\text{ML}} < h < h_{\text{TL}} & \quad h_{\text{norm}} = 1 + (h - h_{\text{ML}})/(h_{\text{TL}} - h_{\text{ML}}) \\ h > h_{\text{TL}} & \quad h_{\text{norm}} = 1 + h/h_{\text{TL}}. \end{aligned} \quad (2)$$

For individual profiles, the mixed layer height was determined by inspection of each profile as the highest altitude at which the virtual potential temperature ( $\Theta_v$ ) was constant (typical variation in the mixed layer was less than 0.5 K) and there was a reduction in the isoprene concentration. The top of the transition layer was defined by a temperature inversion and a rapid decrease in the CO mixing ratio.

The altitude-normalized aggregate profiles of CO (Fig. 7a) and isoprene (Fig. 7b) mixing ratios demonstrate the contrast between the mixed layer and transition layer. During shallow cumulus convection, CO is transported out of the mixed layer into the transition layer due to its longer lifetime relative to isoprene. The modest decrease of CO with altitude in the mixed layer is likely due to the influence of near source emissions in some profiles. In the mixed layer the isoprene profile is variable, and the median is only modestly dependent on altitude with a median mixing ratio of 1 ppbv. However, the median isoprene mixing ratio decreases to  $\sim 10\%$  of this value in the transition layer. The isoprene observed above the mixed layer is consistent with large eddy simulations performed by Kim et al. (2012), who found that cumulus clouds can transport some isoprene out of the mixed layer into the cloud layer.



## 4 Analysis

### 4.1 Aerosol enhancements in the transition layer

During shallow cumulus convection, the air in the transition layer is a mixture of air from the mixed layer below and the free troposphere above. The concentrations of trace gases and extensive aerosol parameters,  $C(h)$ , in the transition layer are described in this analysis by a vertical mixing model consisting of three terms (Eq. 3): a contribution from the mixed layer, a contribution from the free troposphere, and any enhancement  $E(h)$  relative to concentration expected from the vertical mixing alone, as

$$C(h) = C_{\text{ML}}f_{\text{m}}(h) + C_{\text{FT}}(1 - f_{\text{m}}(h)) + E(h), \quad (3)$$

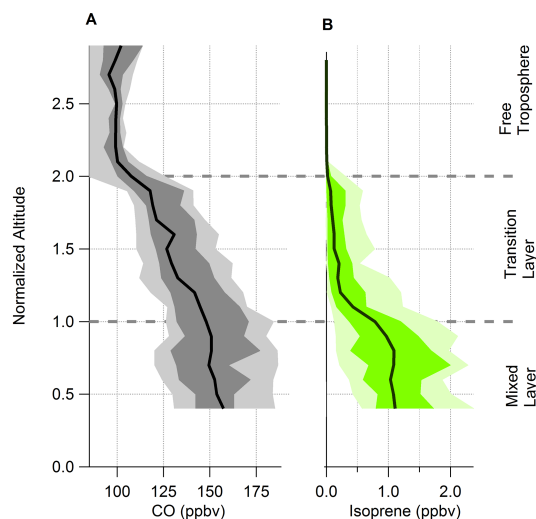
where  $C(h)$  is the aerosol or trace gas concentration, and  $C_{\text{ML}}$  and  $C_{\text{FT}}$  are the aerosol or trace gas concentrations in the mixed layer and the free troposphere. Positive enhancements could be due to local production or direct emissions to the transition layer from buoyant plumes, e.g., large biomass burning sources, and negative enhancements represent losses.

The fraction of air from the mixed layer ( $f_{\text{m}}$ ) present in the transition layer is determined by using the CO mixing ratio as

$$f_{\text{m}}(h) = \frac{\text{CO}(h) - \text{CO}_{\text{FT}}}{\text{CO}_{\text{ML}} - \text{CO}_{\text{FT}}}, \quad (4)$$

for which the enhancement  $E(h)$  due to local production and losses is assumed to be 0. For each profile, the mixing ratio of CO in the mixed layer  $\text{CO}_{\text{ML}}$  and the free troposphere  $\text{CO}_{\text{FT}}$  were determined using the mean between normalized altitudes of 0.5 and 0.9 for the mixed layer and 2.0 and 2.5 for the free troposphere. To investigate transition layer enhancements of chemical concentrations and aerosol extensive properties, we calculate a concentration expected from vertical mixing alone using Eq. (3) and setting  $E(h)$  to 0. The concentration expected from vertical mixing alone is calculated for each profile and aggregated in the same manner as the observations. In Figs. 8–10, the median concentration expected from vertical mixing alone is shown as a dashed line on top of the observed concentrations. The interquartile and interdecile ranges of the value expected from mixing are not shown.

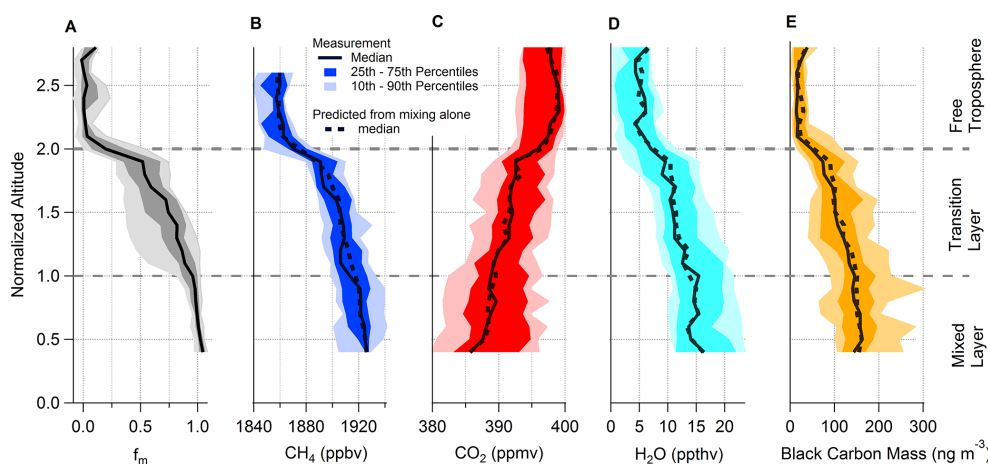
CO is produced through the oxidation of volatile organic compounds, and this CO production likely accounts for a significant fraction of the CO budget during the summer in the SEUS (Hudman et al., 2008). If CO production in the transition layer is significant, the fraction of air from the mixed layer ( $f_{\text{m}}$ , determined using CO) would be biased high and any transition layer enhancements of other species ( $E(h)$ , determined using the CO concentration and Eqs. 3 and 4) would be biased low. By comparing the observed concentration and the concentration expected from vertical mixing alone of several long lifetime species, the importance of CO production in the transition layer can be assessed.



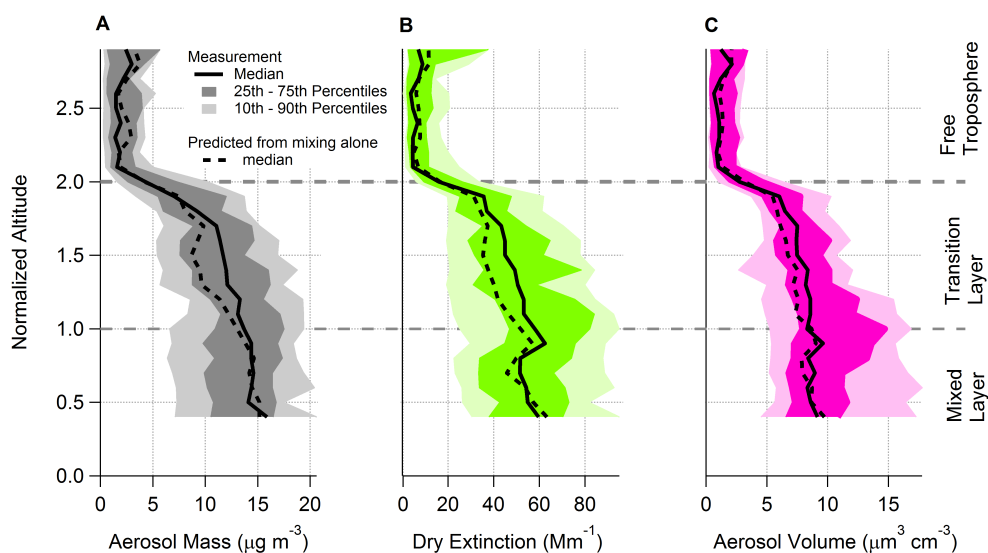
**Figure 7.** Altitude-normalized aggregate profiles of (a) CO; (b) isoprene mixing ratios. The shaded regions show the interdecile range (light) and the interquartile range (medium), and the solid lines are the median (dark).

Figure 8a shows the altitude normalized profile of the fraction of air from the mixed layer ( $f_{\text{m}}$ , calculated using Eq. 4). The median is 1 in the mixed layer, 0 in the free troposphere, and decreases from 1 to 0.6 in the transition layer due to entrainment of air from the free troposphere. Fig. 8b–e show the altitude-normalized aggregate profiles and the median concentration expected from vertical mixing alone (dashed line) of methane ( $\text{CH}_4$ ), carbon dioxide ( $\text{CO}_2$ ), water vapor ( $\text{H}_2\text{O}$ ), and black carbon aerosol mass, respectively. Both  $\text{CH}_4$  and  $\text{CO}_2$  have atmospheric lifetimes greater than 1 year and no significant production or losses in the transition layer on the time scale of atmospheric mixing. (The aggregate profile in Fig. 8b only includes data from the SENEX study because  $\text{CH}_4$  was not measured during SEAC<sup>4</sup>RS.)  $\text{H}_2\text{O}$  and black carbon aerosol are also not produced in the transition layer and are not lost except in the presence of precipitating clouds. Profiles in precipitating clouds are mostly excluded from the aggregate. Based on the agreement between the observed vertical profiles of  $\text{CH}_4$ ,  $\text{CO}_2$ ,  $\text{H}_2\text{O}$ , and black carbon mass (Fig. 8) and their expected concentration from vertical mixing alone, we conclude the CO production in the transition layer is not significant.

In contrast, the altitude-normalized profiles of submicrometer aerosol mass (Fig. 9a), extinction (Fig. 9b), and volume (Fig. 9c) are greater than the value expected from vertical mixing alone (dashed lines) in the transition layer. This indicates that  $E(h)$  is positive for these aerosol properties. These transition layer enhancements are quantified for individual profiles using the difference between the observed value and the value expected from vertical mixing alone. The difference is expressed as a percentage of the observed value and averaged over the transition between normalized altitudes of 1.1



**Figure 8.** Altitude-normalized aggregate profile of (a) fraction of mixed layer air (Eq. 4), (b)  $\text{CH}_4$ , (c),  $\text{CO}_2$ , (d)  $\text{H}_2\text{O}$ , and (e) black carbon aerosol mass. The dashed line shows the concentrations expected from vertical mixing alone (Eq. 3). The shaded regions show the interdecile range (light) and the interquartile range (medium), and the solid lines are the median (dark). These trace gases and black carbon aerosol mass are not expected to be enhanced or reduced in the transition layer. The agreement between the observations and the concentration expected from vertical mixing alone demonstrates that  $\text{CO}$  can be used to quantify the fraction air from the mixed layer.



**Figure 9.** Altitude-normalized aggregate profiles of aerosol mass (a), extinction (b), and volume (c). The aerosol volume was calculated from measured particle size distributions. The shaded regions show the interdecile range (light) and the interquartile range (medium), and the solid lines are the median (dark). The dashed line shows the median value expected from mixing alone (Eq. 3). The difference between the observed median value and the median value expected from mixing alone indicates an enhancement of aerosol in the transition layer.

and 1.9. The mean transition layer enhancements of aerosol mass, extinction, and volume were +8.6, +11.3, and +9.3 %, respectively. The difference in the enhancements of mass, extinction, and volume may reflect actual changes in the aerosol density and extinction cross section or could be due to imperfections in the measurements and data aggregation.

Altitude-normalized aggregate profiles of aerosol composition are shown in Fig. 10. The enhancement of each aerosol component is quantified in the same manner as aerosol mass, extinction, and volume. The observed median is greater than

the value expected from vertical mixing alone by +6 % for OA mass, +18 % for  $\text{SO}_4$ , +25 % for  $\text{NH}_4$ , and +15 % for  $\text{NO}_3$ . Although enhancement of sulfate is larger than OA as a percentage, the absolute enhancement is a similar magnitude for both  $\text{SO}_4$  and OA:  $\sim 0.5 \mu\text{g m}^{-3}$ .

The transition layer enhancements can be further investigated by examining the distribution of enhancements for individual profiles (Fig. 11). For each profile, the enhancement is calculated using the absolute difference between the observed value and that expected from vertical mixing alone.

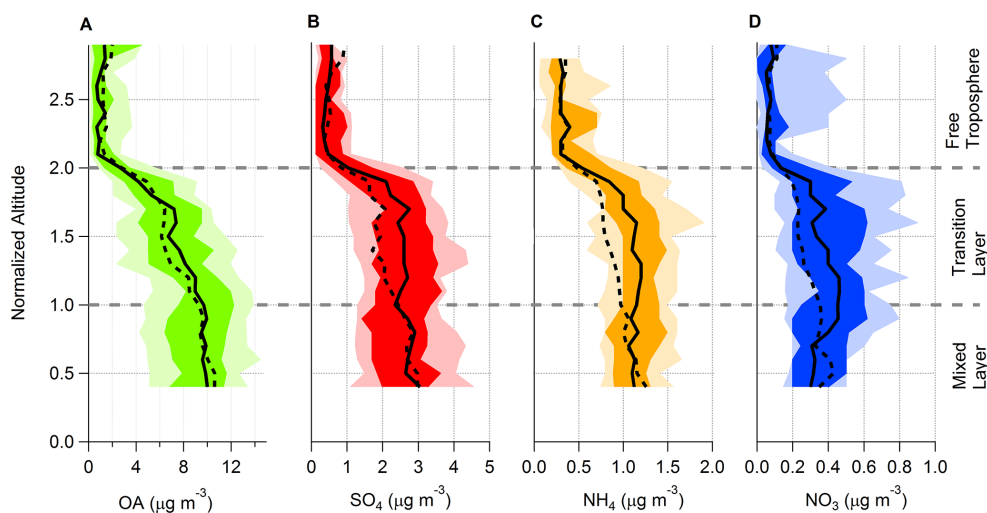


**Figure 10.** Altitude-normalized profiles of the aerosol composition: (a) OA, (b)  $\text{SO}_4$ , (c)  $\text{NH}_4$ , and (d)  $\text{NO}_3$ . The shaded regions show the interdecile range (light) and the interquartile range (medium), and the solid lines are the median (dark). The dashed line shows the median expected concentration from vertical mixing alone (Eq. 3).

The difference is averaged between normalized altitudes of 1.1 and 1.9. Because the distributions of enhancements range from negative to positive values, the Student's  $t$  test is used to assess when the enhancement distributions are statistically different from 0 or without enhancement. Enhancement distributions with  $p$  values less than 0.05 are considered statistically significant. As expected, Fig. 11a–d show conserved species that do not have statistically significant enhancements,  $\text{CH}_4$ ,  $\text{CO}_2$ ,  $\text{H}_2\text{O}$ , and black carbon mass. The enhancement distributions of aerosol mass, extinction, and volume (Fig. 11e–g) are all statistically significant. Although both OA and inorganic aerosol components are enhanced in the transition layer, the enhancement distribution of OA is not statistically significant while the enhancement distribution of inorganic components is significant.

Secondary aerosol formation in the transition layer is the likely mechanism that would lead to the observed enhancement of aerosol mass, volume, and extinction. The enhancement of aerosol loading is the net result of production and loss in the transition layer; however, profiles of black carbon and total sulfur (see Sect. 4.2) suggest that the aerosol losses are small. Secondary aerosol formation in the transition layer is a combination of aqueous production (both in clouds and in aerosol water), homogenous oxidation followed by condensation on existing particles, and condensation of semi-volatile species such as  $\text{NH}_4\text{NO}_3$ . The presence of clouds within the transition layer suggests a large role for aqueous production; however, our data set does not allow us to determine the relative importance of each pathway.

Biomass burning emits aerosol in buoyant plumes that, if large enough, could contribute to the observed enhancement of aerosol loading in the transition layer and would not be consistent with the simple vertical mixing model used here to

describe the transition layer concentrations. Biomass burning is common in the SEUS during the fall, winter, and spring but is less common during the summer. Zhang et al. (2010) found that biomass burning contributed between 2 and 10 % to measurements of  $\text{PM}_{2.5}$  in the summer of 2007 and significantly more in other seasons. Although biomass burning plumes from agricultural fires were transected on level flight legs during both SENEX and SEAC<sup>4</sup>RS, none of the profiles used in this analysis included fresh biomass burning plumes. However, the possibility remains that the aggregate profiles are contaminated by aged and diluted biomass burning plumes which have not been identified. To address this we considered biomass burning emission factors of black carbon, sulfate, and sulfur dioxide ( $\text{SO}_2$ , which is oxidized in the atmosphere to sulfate) reported by Akagi et al. (2011). The emission factors range from 0.20 to  $0.91 \text{ g kg}^{-1}$  for black carbon mass and 0.45 to  $0.87 \text{ g kg}^{-1}$  for the combination of  $\text{SO}_2$  and sulfate. Based on these emission factors, we would expect the ratio of the combination of  $\text{SO}_2$  and sulfate mass to black carbon mass in biomass burning plumes to range from 0.5 to 4.35. If the observed enhancement of sulfate ( $\sim 0.5 \mu\text{g m}^{-3}$ ) were due exclusively to biomass burning, we would expect a concomitant enhancement of black carbon (based on the ratio of emission factors for black carbon and sulfate) in the range of 100 to  $1000 \text{ ng m}^{-3}$ , which is not observed in the profile of black carbon mass (Fig. 8e). Hence, we conclude that the enhancement observed in the altitude-normalized aggregate profile is not due to biomass burning.

## 4.2 Sulfur budget

Further evidence for the transition layer enhancement of particulate sulfate comes from the reduction of the concentration of gas-phase  $\text{SO}_2$  in the transition layer. Particulate sulfate is

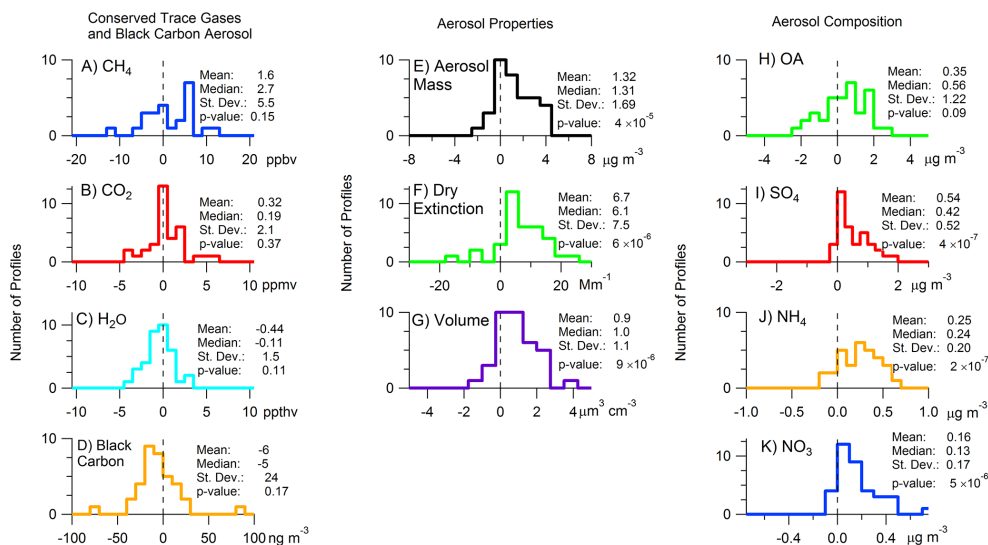


**Figure 11.** Histograms of the transition layer enhancement ( $E(h)$  – see Eq. 4) for several trace gases and aerosol properties. The first column shows conserved species and black carbon: (a) CH<sub>4</sub>, (b) CO<sub>2</sub>, (c) H<sub>2</sub>O, and (d) black carbon mass. The second column shows the aerosol extensive properties: (e) aerosol mass, (f) dry extinction, and (g) aerosol volume. The third column shows the aerosol composition: (h) OA, (i) SO<sub>4</sub>, (j) NH<sub>4</sub>, and (k) NO<sub>3</sub>. The Student's  $t$  test and resulting  $p$  value (noted in each histogram) were used to test whether the mean of each distribution was statistically different from 0.

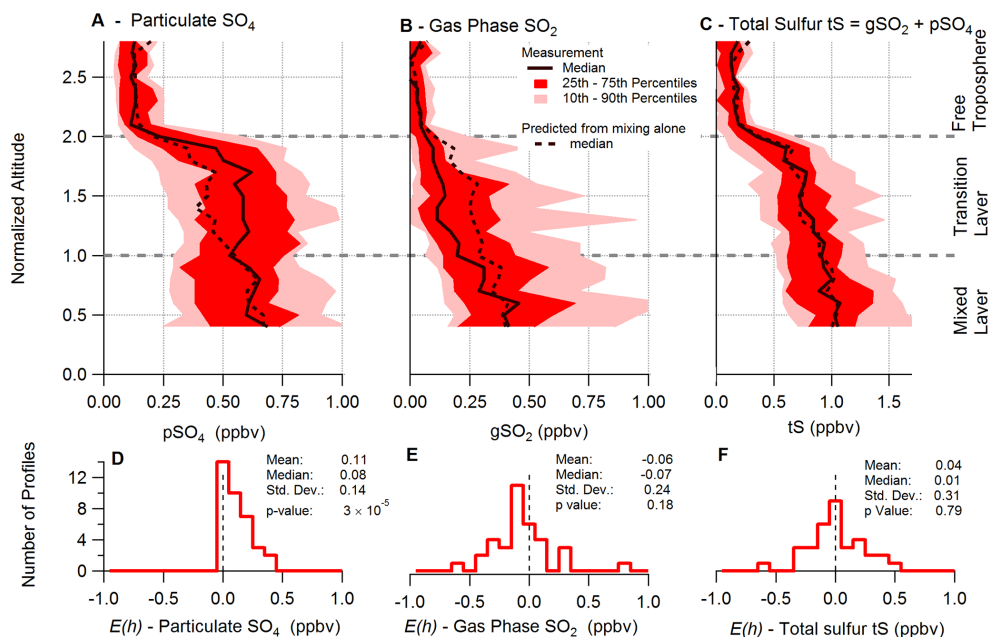


**Figure 12.** Altitude-normalized profiles of (a) particulate sulfate, (b) gas-phase SO<sub>2</sub>, and (c) total sulfur tS. The shaded regions show the interdecile range (light) and the interquartile range (medium), and the solid lines are the median (dark). The dashed line shows the median value expected from mixing alone. Histograms of the transition layer enhancement ( $E(h)$ ) and the results of the  $t$  test for (d) particulate sulfate, (e) SO<sub>2</sub>, and (f) total sulfur are shown.

produced through gas-phase and aqueous oxidation of SO<sub>2</sub> (Seinfeld and Pandis, 1998). We expect that mixing in the transition layer would conserve total sulfur which we define as the sum of particulate sulfate and gas-phase SO<sub>2</sub>. While particulate sulfate is enhanced in the transition layer as de-

scribed in Sect. 4.1, there is also a reduction in the mixing ratio of gas-phase SO<sub>2</sub> in the transition layer. Figure 12a–c show altitude-normalized aggregate profiles and values expected from vertical mixing alone for particulate sulfate, gas-phase SO<sub>2</sub>, and the total sulfur. Particulate sulfate (Fig. 12a)

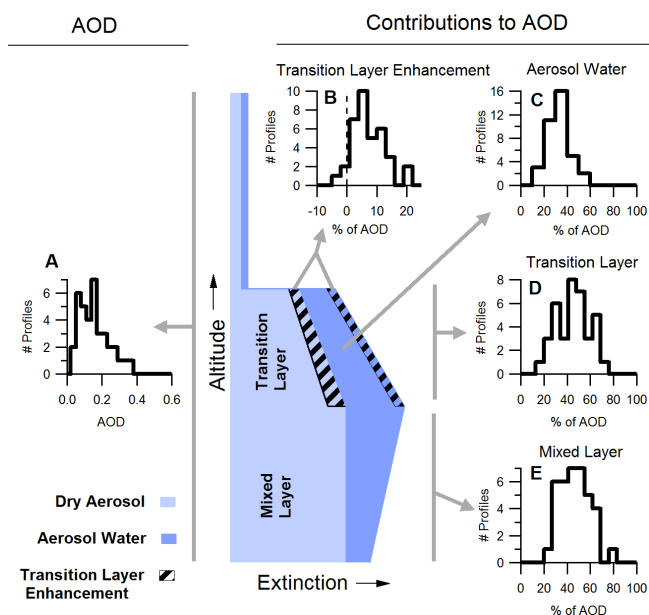


**Figure 13.** The AOD contributions of dry aerosol, aerosol water, and enhanced extinction in the transition layer are illustrated in an idealized profile. The idealized profile of extinction (blue) at the center of the figure shows the vertical location of each contribution to AOD. The light blue area represents the extinction of dry aerosol, and the darker blue area shows the enhancement to aerosol water. The subpanels show (a) histograms of AOD calculated from individual profiles (solid), and the contributions to AOD from the (b) transition layer enhancement of extinction, (c) aerosol water, (d) the transition layer, and (e) the mixed layer. The calculated AOD assumes no contribution from aerosol above the top of the profile and extrapolates the dry extinction and RH to the surface.

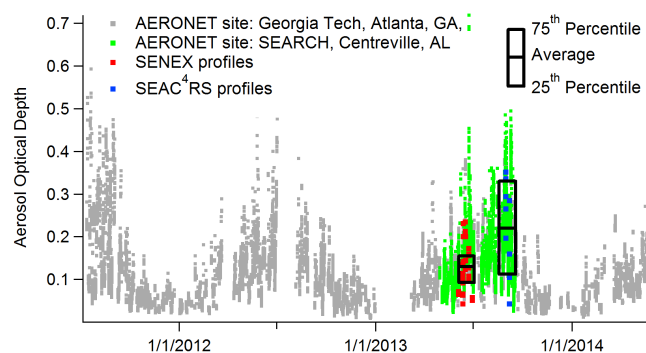


**Figure 14.** The AOD measured by AERONET sun photometers in Atlanta, GA (gray), and Centreville, AL (green), and the AOD from the SENEX (red) and SEAC<sup>4</sup>RS (blue) profiles included in the altitude-normalized aggregate are shown. The black boxes show the average, 25th, and 75th percentiles of AOD from both the SENEX and SEAC<sup>4</sup>RS profiles.

is enhanced by approximately the same amount as the reduction of SO<sub>2</sub> (Fig. 12b): ~0.1 ppbv in the transition layer.

Consequently, the median value of total sulfur agrees well with the value expected from vertical mixing alone.

The enhancement distributions for particulate sulfate, SO<sub>2</sub>, and total sulfur are shown in Fig. 12d–f. While the transition layer enhancement of particulate sulfate is significant with a  $p$  value of  $3 \times 10^{-5}$  (Fig. 12d), the reduction of SO<sub>2</sub> in the transition layer (Fig. 12e) is not. The lack of statistical significance in SO<sub>2</sub> reduction is due to positive outliers in the enhancement distribution. The enhancement distribution of total sulfur indicates a small enhancement that is not statistically significant (Fig. 12f). We note that the conservation of sulfate and SO<sub>2</sub> is only apparent when mixing in the transition layer is taken into account. If biomass burning were the source of the transition layer enhancement of particulate sulfate, we expect that total sulfur would be enhanced a similar magnitude to particulate sulfate in the transition layer.

### 4.3 Aerosol optical depth

Aerosol optical depth is typically measured remotely from space-based satellites (King et al., 1999) and by ground-based sun photometer networks (Holben et al., 2001). These remote measurements of AOD have been complemented by AOD calculated from aircraft-based in situ measurements of extinction which have the ability to quantify contributions to the AOD from individual layers and aerosol water (Crumeyrolle et al., 2014; Esteve et al., 2012). Calculated from in situ measurements, AOD is the integral of the ambient aerosol extinction coefficient ( $\sigma_{\text{ext}}$ ):

$$\text{AOD} = \int_{\text{surface}}^{\text{TOA}} \sigma_{\text{ext}}(z) dz, \quad (5)$$

where  $\sigma_{\text{ext}}$  is a function of altitude  $z$  and the integration extends to the top of the atmosphere (TOA). The extinction coefficient in Eq. (5) is at ambient relative humidity, pressure, and temperature. Several assumptions are necessary to calculate ambient extinction and subsequently AOD. First, the aircraft profiles of dry extinction, relative humidity, pressure, and temperature must be extrapolated to the surface. Because extinction at the surface and aloft in the mixed layer are correlated (Fig. 4), the dry extinction is extrapolated as a constant to the surface based on the mean extinction measured in the lowest 200 m of each profile. Relative humidity is extrapolated to the surface using the linear trend in the lowest 200 m of each profile when the trend is positive (RH increases with increasing altitude); otherwise, it is extrapolated as a constant based on the mean RH of the lowest 200 m of each profile. Pressure and temperature are both extrapolated using the linear trend in the lowest 200 m of each profile. The second assumption is that the contributions to AOD from aerosol layers above the top of the aircraft profile are negligible. For example, smoke from large forest fires in the western US can be lofted high into the troposphere and transported over the SEUS (Peltier et al., 2007). This contribution to AOD

could not be included if the smoke layer were above the maximum altitude of the profile. In this case the AOD calculated from the in situ profiles is a lower limit. Third, we neglect the contribution to the AOD from supermicrometer particles, which we estimate to be less than 10 % of the sub-micrometer AOD based on coarse particle size distribution measurements made during both SENEX and SEAC<sup>4</sup>RS. Fourth, because we have restricted calculated aerosol hygroscopic growth to RH values less than 95 %, the AOD calculated here is only a lower limit.

In addition to the AOD for each profile in the altitude-normalized aggregate, we have also calculated the contributions to AOD from the mixed layer, the transition layer, aerosol water, and the enhancement of aerosol extinction in the transition layer. The median calculated AOD was 0.14 and the IQR spanned 0.10 to 0.20 (Fig. 13a). An idealized profile of extinction during shallow cumulus convection is used to show the contributions to AOD from the transition layer enhancement of extinction (Fig. 13b), aerosol water (Fig. 13c), the transition layer (Fig. 13d), and the mixed layer (Fig. 13e). The contribution of the transition layer enhancement of ambient extinction (median: 7 %, IQR: 4–10 %) is split between the enhancement of dry extinction and the aerosol water associated with the additional aerosol loading. The contribution of aerosol water to the whole profile (median: 33 %, IQR: 24–38 %) is sensitive to the aerosol hygroscopicity parameter and ambient RH encountered. The transition layer contribution (median: 45 %, IQR: 33–55 %) was slightly smaller than the mixed layer contribution (median: 48 %, IQR: 38–57 %). The mixed layer's slightly greater vertical extent and higher average dry extinction favor a larger contribution to AOD; however, the transition layer also provides a substantial contribution to AOD because of the aerosol water associated with the higher mean RH in the transition layer. The contributions to AOD presented in Fig. 13 have substantial overlap (i.e., aerosol water also contributes to mixed and transition layer AOD); hence, the contributions do not add to unity.

The altitude-normalized aggregate profiles used in this analysis are drawn from 37 vertical profiles; however, they represent only eight afternoons during the summer of 2013. For comparison and context, Fig. 14 shows an extended time series of 532 nm AOD (level 2 data) measured by AERONET sun photometers (Holben et al., 2001) at the Centreville SEARCH site and at the Georgia Tech site in Atlanta, Georgia. The Georgia Tech site is in an urban area and is perhaps biased toward larger AOD from urban emissions, while the Centreville site is rural. The sun photometers only report data during cloud-free conditions. Plotted on top of these data from the sun photometers are the AOD from the profiles used in the altitude-normalized aggregate. These data are grouped into the profiles from the SENEX and SEAC<sup>4</sup>RS studies. Aircraft profiles during the SENEX study did not sample AOD greater than 0.3 while the maximum of AOD observed by the sun photometers was greater than 0.4. Profiles during the

SEAC<sup>4</sup>RS study, although limited in number, cover a range of AOD similar to the sun photometers. Because the majority of the profiles in the altitude-normalized aggregate are from the SENEX study, the aggregate may be biased toward cleaner conditions. The range of AOD observed during summers of 2011–2013 at the Georgia Tech site indicate that the summer of 2013 is not an outlier with AOD higher or lower than typical summers. This is consistent with the analysis of Kim et al. (2015), who has compared satellite measurements of AOD during the summers 2006–2013.

Several SEUS studies have noted decreases in anthropogenic emissions (sulfur, nitrogen oxides, and volatile organic compounds) in the first decade of the 21st century (Alston et al., 2012; Attwood et al., 2014; Hand et al., 2012, 2013). Concurrently, particulate sulfate, OA, and AOD have also decreased. Alston et al. (2012) have shown that the summertime mean AOD over Georgia reported by the MISR instrument on the Terra spacecraft decreased from  $\sim 0.3$  in the summer of 2000 to less than 0.2 in the summer of 2009, which is in the range of AOD calculated in this work for the summer 2013.

## 5 Conclusions

Several preceding studies have observed vertical transport of trace gases and aerosol from the mixed layer into the cloud-influenced transition layer during shallow cumulus convection (Angevine, 2005; Ching and Alkezweeny, 1986; Greenhut, 1986; Langford et al., 2010). Our observations are consistent with this earlier work. In addition to vertical transport and redistribution of aerosol, we observed a modest enhancement of aerosol loading in the transition layer and conclude that secondary aerosol formation in the transition layer is the likely source of the enhancement. Although we cannot distinguish between condensational and aqueous aerosol formation pathways, the presence of clouds and elevated relative humidity in the transition layer suggests a potential role for aqueous reactions. Using measurements of particulate oxalate as a tracer for aqueous processing, Wonaschuetz et al. (2012) and Sorooshian et al. (2007) have also observed evidence for secondary aerosol formation in the transition layer during cumulus convection over Texas and near the coast of California. Wonaschuetz et al. (2012) show no trends in the OA and particulate sulfate mass fractions with altitude in the mixed and transition layers, which could occur if the production were sufficiently small or if the additional aerosol mass in the transition layer were produced with the same ratio of OA and particulate sulfate that was originally present in the mixed layer. In contrast, our measurements show a distinct difference in composition between the mixed and transition layers and imply a similar magnitude of secondary sulfate and OA production in the transition layer, although the production of OA was not statistically significant.

Goldstein et al. (2009) and Ford and Heald (2013) hypothesized a layer of aerosol that would be sufficient to explain a significant fraction of the observed summertime enhancement of AOD (2–3 times greater than winter) and that does not contribute to aerosol mass at the surface. The hypothesis is partially supported by the spatial similarity of summertime biogenic emission and summertime AOD over the SEUS. However, Alston et al. (2012) found that the spatial similarity depended on the spatial resolution AOD of the data used in the analysis, and their analysis of AOD and surface aerosol mass over Georgia did not fully support the hypothesis. Kim et al. (2015) found that the increase of the planetary boundary layer height during the summer could bring the seasonality of the AOD and surface aerosol mass into agreement without the need for an enhanced aerosol layer aloft.

Here, we have examined in situ vertical profiles of aerosol and found the dry aerosol to be well mixed in the lowest layer. Above the lowest layer, the aerosol mass and extinction decreased with increasing altitude above that layer (Figs. 3–5). The hygroscopic growth of aerosol at high RH resulted in a layer of enhanced extinction near the top of the mixed layer. The aerosol water accounted for approximately a third of the AOD which would explain a portion of the summertime AOD enhancement. The hypothesized, large enhancement of secondary aerosol aloft was not apparent in these aggregate profiles. However, after normalizing the altitude to the vertical structure and using the CO concentration to quantify the vertical mixing (Figs. 7–10), we were able to resolve a modest enhancement of aerosol in the transition layer. This layer was not consistent with the hypothesized layer in magnitude, and the observed composition was not consistent with the SOA dominated layer hypothesized by Goldstein et al. (2009). We observed enhancements that were less than 10% of AOD, and sulfate and OA were enhanced by similar magnitude although the OA enhancement was not statistically significant. The seasonality of the enhancement of surface aerosol mass (less than 1.6 times greater in summer than winter) compared to the AOD enhancement (2–3 times) was the primary evidence for the hypothesized layer. Given the absence of such a layer, our observations suggest that other factors such as meteorology and transport may influence the seasonality of the relationship of AOD to surface aerosol mass and warrant further investigation.

*Acknowledgements.* We thank the NOAA WP-3D and NASA DC-8 scientists, flight crews, and support staff for their outstanding efforts in the field. In particular we would like to thank M. K. Trainer for flight planning during SENEX. Isoprene measurements during SEAC<sup>4</sup>RS were supported by BMVIT/FFG-ALR in the frame of the Austrian Space Application Program (ASAP 8, project 833451). PCJ, DAD, and JLJ measured aerosol mass and composition during SEAC<sup>4</sup>RS and were supported by NASA NNX12AC03G and NSF AGS-1243354. Additionally, the SEARCH aerosol network provided surface measurement used in overflight comparisons, and we thank Brent Holben and Brad Gingrey and their staff for

establishing and maintaining the Centreville AERONET sites used in this investigation. This analysis is funded by the NOAA's Health of the Atmosphere Program and Atmospheric Chemistry, Carbon Cycles, and Climate Program and by NASA's Radiation Sciences Program under Award NNX12AT31I.

Edited by: A. Petzold

## References

- Akagi, S. K., Yokelson, R. J., Wiedinmyer, C., Alvarado, M. J., Reid, J. S., Karl, T., Crounse, J. D., and Wennberg, P. O.: Emission factors for open and domestic biomass burning for use in atmospheric models, *Atmos. Chem. Phys.*, 11, 4039–4072, doi:10.5194/acp-11-4039-2011, 2011.
- Alston, E. J., Sokolik, I. N., and Kalashnikova, O. V.: Characterization of atmospheric aerosol in the US Southeast from ground- and space-based measurements over the past decade, *Atmos. Meas. Tech.*, 5, 1667–1682, doi:10.5194/amt-5-1667-2012, 2012.
- Angevine, W. M.: An integrated turbulence scheme for boundary layers with shallow cumulus applied to pollutant transport, *J. Appl. Meteorol.*, 44, 1436, doi:10.1175/jam2284.1, 2005.
- Attwood, A. R., Washenfelder, R. A., Brock, C. A., Hu, W., Baumann, K., Campuzano-Jost, P., Day, D. A., Edgerton, E. S., Murphy, D. M., Palm, B. B., McComiskey, A., Wagner, N. L., de Sá, S. S., Ortega, A., Martin, S. T., Jimenez, J. L., and Brown, S. S.: Trends in sulfate and organic aerosol mass in the Southeast U.S.: Impact on aerosol optical depth and radiative forcing, *Geophys. Res. Lett.*, 41, 7701, doi:10.1002/2014GL061669, 2014.
- Bahreini, R., Dunlea, E. J., Matthew, B. M., Simons, C., Docherty, K. S., DeCarlo, P. F., Jimenez, J. L., Brock, C. A., and Middlebrook, A. M.: Design and operation of a pressure-controlled inlet for airborne sampling with an aerodynamic aerosol lens, *Aerosol Sci. Tech.*, 42, 465, doi:10.1080/02786820802178514, 2008.
- Bahreini, R., Ervens, B., Middlebrook, A. M., Warneke, C., de Gouw, J. A., DeCarlo, P. F., Jimenez, J. L., Brock, C. A., Neuman, J. A., Ryerson, T. B., Stark, H., Atlas, E., Brioude, J., Fried, A., Holloway, J. S., Peischl, J., Richter, D., Walega, J., Weibring, P., Wollny, A. G., and Fehsenfeld, F. C.: Organic aerosol formation in urban and industrial plumes near Houston and Dallas, Texas, *J. Geophys. Res.-Atmos.*, 114, D00F16, doi:10.1029/2008jd011493, 2009.
- Bergstrom, R. W., Russell, P. B., and Hignett, P.: Wavelength dependence of the absorption of black carbon particles: Predictions and results from the TARFOX experiment and implications for the aerosol single scattering albedo, *J. Atmos. Sci.*, 59, 567, doi:10.1175/1520-0469(2002)059<0567:wdotao>2.0.CO;2, 2002.
- Brock, C. A., Wagner, N. L., Anderson, B. E., Beyersdorf, A., Campuzano-Jost, P., Carlton, A. G., Day, D. A., Diskin, G. S., Gordon, T. D., Jimenez, J. L., Lack, D. A., Liao, J., Markovic, M. Z., Middlebrook, A. M., Perring, A., Richardson, M. S., Schwarz, J. P., Washenfelder, R. A., Welti, A., Ziemba, L., and Murphy, D. M.: Aerosol Optical Properties in the Southeastern United States in Summer – Part I: Hygroscopic Growth, in preparation, 2015.
- Cai, Y., Montague, D. C., Mooiweer-Bryan, W., and Deshler, T.: Performance characteristics of the ultra high sen-

- sitivity aerosol spectrometer for particles between 55 and 800 nm: Laboratory and field studies, *J. Aerosol Sci.*, 39, 759, doi:10.1016/j.jaerosci.2008.04.007, 2008.
- Canagaratna, M. R., Jayne, J. T., Jimenez, J. L., Allan, J. D., Alfarra, M. R., Zhang, Q., Onasch, T. B., Drewnick, F., Coe, H., Middlebrook, A., Delia, A., Williams, L. R., Trimborn, A. M., Northway, M. J., DeCarlo, P. F., Kolb, C. E., Davidovits, P., and Worsnop, D. R.: Chemical and microphysical characterization of ambient aerosols with the aerodyne aerosol mass spectrometer, *Mass Spectrom. Rev.*, 26, 185, doi:10.1002/mas.20115, 2007.
- Carlton, A. G. and Turpin, B. J.: Particle partitioning potential of organic compounds is highest in the Eastern US and driven by anthropogenic water, *Atmos. Chem. Phys.*, 13, 10203–10214, doi:10.5194/acp-13-10203-2013, 2013.
- Carlton, A. G., Turpin, B. J., Altieri, K. E., Seitzinger, S. P., Mathur, R., Roselle, S. J., and Weber, R. J.: CMAQ Model Performance Enhanced When In-Cloud Secondary Organic Aerosol is Included: Comparisons of Organic Carbon Predictions with Measurements, *Environ. Sci. Tech.*, 42, 8798, doi:10.1021/es801192n, 2008.
- Ching, J. K. S. and Alkezweeny, A. J.: Tracer Study of Vertical Exchange by Cumulus Clouds, *J. Clim. Appl. Meteorol.*, 25, 1702, doi:10.1175/1520-0450(1986)025<1702:tsoveb>2.0.co;2, 1986.
- Ching, J. K. S., Shipley, S. T., and Browell, E. V.: Evidence for Cloud Venting of Mixed Layer Ozone and Aerosols, *Atmos. Environ.*, 22, 225, doi:10.1016/0004-6981(88)90030-3, 1988.
- Crumeyrolle, S., Chen, G., Ziemba, L., Beyersdorf, A., Thornhill, L., Winstead, E., Moore, R. H., Shook, M. A., Hudgins, C., and Anderson, B. E.: Factors that influence surface PM<sub>2.5</sub> values inferred from satellite observations: perspective gained for the US Baltimore-Washington metropolitan area during DISCOVER-AQ, *Atmos. Chem. Phys.*, 14, 2139–2153, doi:10.5194/acp-14-2139-2014, 2014.
- de Gouw, J. A. and Warneke, C.: Measurements of volatile organic compounds in the earth's atmosphere using proton-transfer-reaction mass spectrometry, *Mass Spectrom. Rev.*, 26, 223, doi:10.1002/mas.20119, 2007.
- de Gouw, J. A. and Jimenez, J. L.: Organic Aerosols in the Earth's Atmosphere, *Environ. Sci. Tech.*, 43, 7614, doi:10.1021/es9006004, 2009.
- Drewnick, F., Hings, S. S., DeCarlo, P., Jayne, J. T., Gonin, M., Fuhrer, K., Weimer, S., Jimenez, J. L., Demerjian, K. L., Borrmann, S., and Worsnop, D. R.: A new time-of-flight aerosol mass spectrometer (TOF-AMS) – Instrument description and first field deployment, *Aerosol Sci. Tech.*, 39, 637, doi:10.1080/02786820500182040, 2005.
- Dunlea, E. J., DeCarlo, P. F., Aiken, A. C., Kimmel, J. R., Peltier, R. E., Weber, R. J., Tomlinson, J., Collins, D. R., Shinzuka, Y., McNaughton, C. S., Howell, S. G., Clarke, A. D., Emmons, L. K., Apel, E. C., Pfister, G. G., van Donkelaar, A., Martin, R. V., Millet, D. B., Heald, C. L., and Jimenez, J. L.: Evolution of Asian aerosols during transpacific transport in INTEX-B, *Atmos. Chem. Phys.*, 9, 7257–7287, doi:10.5194/acp-9-7257-2009, 2009.
- Eatough, D. J., Caka, F. M., and Farber, R. J.: The Conversion of SO<sub>2</sub> to Sulfate in the Atmosphere, *Isr. J. Chem.*, 34, 301, doi:10.1002/ijch.199400034, 1994.
- Edgerton, E. S., Hartsell, B. E., Saylor, R. D., Jansen, J. J., Hansen, D. A., and Hidy, G. M.: The Southeastern Aerosol Research and Characterization Study: Part II. Filter-based Measurements of Fine and Coarse Particulate Matter Mass and Composition, *J. Air Waste Manage.*, 55, 1527, doi:10.1080/10473289.2005.10464744, 2005.
- Edgerton, E. S., Hartsell, B. E., Saylor, R. D., Jansen, J. J., Hansen, D. A., and Hidy, G. M.: The Southeastern Aerosol Research and Characterization Study, Part 3: Continuous Measurements of Fine Particulate Matter Mass and Composition, *J. Air Waste Manage.*, 56, 1325, doi:10.1080/10473289.2006.10464585, 2006.
- Ervens, B., Turpin, B. J., and Weber, R. J.: Secondary organic aerosol formation in cloud droplets and aqueous particles (aqSOA): a review of laboratory, field and model studies, *Atmos. Chem. Phys.*, 11, 11069–11102, doi:10.5194/acp-11-11069-2011, 2011.
- Esteve, A. R., Ogren, J. A., Sheridan, P. J., Andrews, E., Holben, B. N., and Utrillas, M. P.: Sources of discrepancy between aerosol optical depth obtained from AERONET and in-situ aircraft profiles, *Atmos. Chem. Phys.*, 12, 2987–3003, doi:10.5194/acp-12-2987-2012, 2012.
- Ford, B. and Heald, C. L.: Aerosol loading in the Southeastern United States: reconciling surface and satellite observations, *Atmos. Chem. Phys.*, 13, 9269–9283, doi:10.5194/acp-13-9269-2013, 2013.
- Goldstein, A. H., Koven, C. D., Heald, C. L., and Fung, I. Y.: Biogenic carbon and anthropogenic pollutants combine to form a cooling haze over the southeastern United States, *P. Natl. Acad. Sci. USA*, 106, 8835, doi:10.1073/pnas.0904128106, 2009.
- Greenhut, G. K.: Transport of Ozone Between Boundary-Layer and Cloud Layer by Cumulus Clouds, *J. Geophys. Res.-Atmos.*, 91, 8613, doi:10.1029/JD091iD08p08613, 1986.
- Hand, J. L., Schichtel, B. A., Malm, W. C., and Pitchford, M. L.: Particulate sulfate ion concentration and SO<sub>2</sub> emission trends in the United States from the early 1990s through 2010, *Atmos. Chem. Phys.*, 12, 10353–10365, doi:10.5194/acp-12-10353-2012, 2012.
- Hand, J. L., Schichtel, B. A., Malm, W. C., and Frank, N. H.: Spatial and Temporal Trends in PM<sub>2.5</sub> Organic and Elemental Carbon across the United States, *Adv. Meteorol.*, 367674, doi:10.1155/2013/367674, 2013.
- Hansen, D. A., Edgerton, E. S., Hartsell, B. E., Jansen, J. J., Kandasamy, N., Hidy, G. M., and Blanchard, C. L.: The Southeastern Aerosol Research and Characterization Study: Part 1-Overview, *J. Air Waste Manage.*, 53, 1460, doi:10.1080/10473289.2003.10466318, 2003.
- He, C., Liu, J., Carlton, A. G., Fan, S., Horowitz, L. W., Levy, H., II, and Tao, S.: Evaluation of factors controlling global secondary organic aerosol production from cloud processes, *Atmos. Chem. Phys.*, 13, 1913–1926, doi:10.5194/acp-13-1913-2013, 2013.
- Hoff, R. M. and Christopher, S. A.: Remote Sensing of Particulate Pollution from Space: Have We Reached the Promised Land?, *J. Air Waste Manage.*, 59, 645, doi:10.3155/1047-3289.59.6.645, 2009.
- Holben, B. N., Tanre, D., Smirnov, A., Eck, T. F., Slutsker, I., Abuhassan, N., Newcomb, W. W., Schafer, J. S., Chatenet, B., Lavenue, F., Kaufman, Y. J., Castle, J. V., Setzer, A., Markham, B., Clark, D., Frouin, R., Halthore, R., Karneli, A., O'Neill, N. T., Pietras, C., Pinker, R. T., Voss, K., and Zibordi, G.: An emerging ground-based aerosol climatology: Aerosol optical



- depth from AERONET, *J. Geophys. Res.-Atmos.*, 106, 12067, doi:10.1029/2001jd900014, 2001.
- Holloway, J. S., Jakoubek, R. O., Parrish, D. D., Gerbig, C., Volz-Thomas, A., Schmitgen, S., Fried, A., Wert, B., Henry, B., and Drummond, J. R.: Airborne intercomparison of vacuum ultraviolet fluorescence and tunable diode laser absorption measurements of tropospheric carbon monoxide, *J. Geophys. Res.-Atmos.*, 105, 24251, doi:10.1029/2000jd900237, 2000.
- Hudman, R. C., Murray, L. T., Jacob, D. J., Millet, D. B., Turquety, S., Wu, S., Blake, D. R., Goldstein, A. H., Holloway, J., and Sachse, G. W.: Biogenic versus anthropogenic sources of CO in the United States, *Geophys. Res. Lett.*, 35, L04801, doi:10.1029/2007gl032393, 2008.
- Kim, P. S., Jacob, D. J., Fisher, J. A., Travis, K., Yu, K., Zhu, L., Yantosca, R. M., Sulprizio, M. P., Jimenez, J. L., Campuzano-Jost, P., Froyd, K. D., Liao, J., Hair, J. W., Fenn, M. A., Butler, C. F., Wagner, N. L., Brock, C. A., Gordon, T. D., Welti, A., O., W. P., Crounse, J. D., St. Clair, J. M., Teng, A. P., Millet, D. B., Schwarz, J. P., Markovic, M. Z., and Perring, A. E.: Sources, seasonality, and trends of Southeast US aerosol: an integrated analysis of surface, aircraft, and satellite observations with the GEOS-Chem chemical transport model, *Atmos. Chem. Phys. Discuss.*, submitted, 2015.
- Kim, S., Huey, L. G., Stickel, R. E., Tanner, D. J., Crawford, J. H., Olson, J. R., Chen, G., Brune, W. H., Ren, X., Leshner, R., Wooldridge, P. J., Bertram, T. H., Perring, A., Cohen, R. C., Lefter, B. L., Shetter, R. E., Avery, M., Diskin, G., and Sokolik, I.: Measurement of HO<sub>2</sub>NO<sub>2</sub> in the free troposphere during the intercontinental chemical transport experiment – North America 2004, *J. Geophys. Res.-Atmos.*, 112, D12S01, doi:10.1029/2006jd007676, 2007.
- Kim, S. W., Barth, M. C., and Trainer, M.: Influence of fair-weather cumulus clouds on isoprene chemistry, *J. Geophys. Res.-Atmos.*, 117, D10302, doi:10.1029/2011jd017099, 2012.
- King, M. D., Kaufman, Y. J., Tanre, D., and Nakajima, T.: Remote sensing of tropospheric aerosols from space: Past, present, and future, *B. Am. Meteorol. Soc.*, 80, 2229, doi:10.1175/1520-0477(1999)080<2229:rsotaf>2.0.co;2, 1999.
- Lack, D. A. and Langridge, J. M.: On the attribution of black and brown carbon light absorption using the Angstrom exponent, *Atmos. Chem. Phys.*, 13, 10535–10543, doi:10.5194/acp-13-10535-2013, 2013.
- Langford, A. O., Tucker, S. C., Senff, C. J., Banta, R. M., Brewer, W. A., Alvarez, R. J., Hardesty, R. M., Lerner, B. M., and Williams, E. J.: Convective venting and surface ozone in Houston during TexAQS 2006, *J. Geophys. Res.-Atmos.*, 115, D16305, doi:10.1029/2009jd013301, 2010.
- Langridge, J. M., Richardson, M. S., Lack, D., Law, D., and Murphy, D. M.: Aircraft Instrument for Comprehensive Characterization of Aerosol Optical Properties, Part I: Wavelength-Dependent Optical Extinction and Its Relative Humidity Dependence Measured Using Cavity Ringdown Spectroscopy, *Aerosol Sci. Tech.*, 45, 1305, doi:10.1080/02786826.2011.592745, 2011.
- Luria, M. and Sievering, H.: Heterogeneous and Homogeneous Oxidation of SO<sub>2</sub> in the Marine Atmosphere, *Atmos. Environ.*, 25, 1489, doi:10.1016/0960-1686(91)90008-u, 1991.
- Massoli, P., Bates, T. S., Quinn, P. K., Lack, D. A., Baynard, T., Lerner, B. M., Tucker, S. C., Brioude, J., Stohl, A., and Williams, E. J.: Aerosol optical and hygroscopic properties during TexAQS-GoMACCS 2006 and their impact on aerosol direct radiative forcing, *J. Geophys. Res.-Atmos.*, 114, D00F07, doi:10.1029/2008jd011604, 2009.
- McKeen, S., Chung, S. H., Wilczak, J., Grell, G., Djalalova, I., Peckham, S., Gong, W., Bouchet, V., Moffet, R., Tang, Y., Carmichael, G. R., Mathur, R., and Yu, S.: Evaluation of several PM<sub>2.5</sub> forecast models using data collected during the ICARTT/NEAQS 2004 field study, *J. Geophys. Res.-Atmos.*, 112, D10S20, doi:10.1029/2006jd007608, 2007.
- McNaughton, C. S., Clarke, A. D., Howell, S. G., Pinkerton, M., Anderson, B., Thornhill, L., Hudgins, C., Winstead, E., Dibb, J. E., Scheuer, E., and Maring, H.: Results from the DC-8 Inlet Characterization Experiment (DICE): Airborne versus surface sampling of mineral dust and sea salt aerosols, *Aerosol Sci. Tech.*, 41, 136, doi:10.1080/02786820601118406, 2007.
- Middlebrook, A. M., Bahreini, R., Jimenez, J. L., and Canagaratna, M. R.: Evaluation of Composition-Dependent Collection Efficiencies for the Aerodyne Aerosol Mass Spectrometer using Field Data, *Aerosol Sci. Tech.*, 46, 258, doi:10.1080/02786826.2011.620041, 2012.
- Peischl, J., Ryerson, T. B., Holloway, J. S., Trainer, M., Andrews, A. E., Atlas, E. L., Blake, D. R., Daube, B. C., Dlugokencky, E. J., Fischer, M. L., Goldstein, A. H., Guha, A., Karl, T., Kofler, J., Kosciuch, E., Misztal, P. K., Perring, A. E., Pollack, I. B., Santoni, G. W., Schwarz, J. P., Spackman, J. R., Wofsy, S. C., and Parrish, D. D.: Airborne observations of methane emissions from rice cultivation in the Sacramento Valley of California, *J. Geophys. Res.-Atmos.*, 117, D00V25, doi:10.1029/2012jd017994, 2012.
- Peltier, R. E., Sullivan, A. P., Weber, R. J., Brock, C. A., Wollny, A. G., Holloway, J. S., de Gouw, J. A., and Warneke, C.: Fine aerosol bulk composition measured on WP-3D research aircraft in vicinity of the Northeastern United States – results from NEAQS, *Atmos. Chem. Phys.*, 7, 3231–3247, doi:10.5194/acp-7-3231-2007, 2007.
- Petters, M. D. and Kreidenweis, S. M.: A single parameter representation of hygroscopic growth and cloud condensation nucleus activity, *Atmos. Chem. Phys.*, 7, 1961–1971, doi:10.5194/acp-7-1961-2007, 2007.
- Quinn, P. K., Bates, T. S., Baynard, T., Clarke, A. D., Onasch, T. B., Wang, W., Rood, M. J., Andrews, E., Allan, J., Carrico, C. M., Coffman, D., and Worsnop, D.: Impact of particulate organic matter on the relative humidity dependence of light scattering: A simplified parameterization, *Geophys. Res. Lett.*, 32, L22809, doi:10.1029/2005gl024322, 2005.
- Ryerson, T. B., Buhr, M. P., Frost, G. J., Goldan, P. D., Holloway, J. S., Hubler, G., Jobson, B. T., Kuster, W. C., McKeen, S. A., Parrish, D. D., Roberts, J. M., Sueper, D. T., Trainer, M., Williams, J., and Fehsenfeld, F. C.: Emissions lifetimes and ozone formation in power plant plumes, *J. Geophys. Res.-Atmos.*, 103, 22569, doi:10.1029/98jd01620, 1998.
- Sachse, G. W., Hill, G. F., Wade, L. O., and Perry, M. G.: Fast Response, High Precision Carbon Monoxide Sensor Using a Tunable Diode-Laser Absorption Technique, *J. Geophys. Res.-Atmos.*, 92, 2071, doi:10.1029/JD092iD02p02071, 1987.
- Santarpia, J. L., Li, R. J., and Collins, D. R.: Direct measurement of the hydration state of ambient aerosol populations, *J. Geophys. Res.-Atmos.*, 109, D18209, doi:10.1029/2004jd004653, 2004.

- Schwarz, J. P., Gao, R. S., Spackman, J. R., Watts, L. A., Thomson, D. S., Fahey, D. W., Ryerson, T. B., Peischl, J., Holloway, J. S., Trainer, M., Frost, G. J., Baynard, T., Lack, D. A., de Gouw, J. A., Warneke, C., and Del Negro, L. A.: Measurement of the mixing state, mass, and optical size of individual black carbon particles in urban and biomass burning emissions, *Geophys. Res. Lett.*, 35, L13810, doi:10.1029/2008gl033968, 2008.
- Seinfeld, J. H. and Pandis, S. N.: *Atmospheric Chemistry and Physics*, John Wiley & Sons, New York, 817–821, 1998.
- Siebesma, A. P.: Shallow Cumulus Convection, in: *Buoyant Convection in Geophysical Flows*, edited by: Plate, E. J., Fedorovich, E. E., Viegas, D. X., and Wyngaard, J. C., Kluwer Academic Publishers, Dordrecht, 441–486, 1998.
- Sorooshian, A., Varutbangkul, V., Brechtel, F. J., Ervens, B., Feingold, G., Bahreini, R., Murphy, S. M., Holloway, J. S., Atlas, E. L., Buzorius, G., Jonsson, H., Flagan, R. C., and Seinfeld, J. H.: Oxalic acid in clear and cloudy atmospheres: Analysis of data from International Consortium for Atmospheric Research on Transport and Transformation 2004, *J. Geophys. Res.-Atmos.*, 111, D23S45, doi:10.1029/2005jd006880, 2006.
- Sorooshian, A., Lu, M.-L., Brechtel, F. J., Jonsson, H., Feingold, G., Flagan, R. C., and Seinfeld, J. H.: On the source of organic acid aerosol layers above clouds, *Environ. Sci. Tech.*, 41, 4647, doi:10.1021/es0630442, 2007.
- Vay, S. A., Choi, Y., Vadrevu, K. P., Blake, D. R., Tyler, S. C., Wisthaler, A., Hecobian, A., Kondo, Y., Diskin, G. S., Sachse, G. W., Woo, J. H., Weinheimer, A. J., Burkhardt, J. F., Stohl, A., and Wennberg, P. O.: Patterns of CO<sub>2</sub> and radiocarbon across high northern latitudes during International Polar Year 2008, *J. Geophys. Res.-Atmos.*, 116, D14301, doi:10.1029/2011jd015643, 2011.
- Warren, S. G., Eastman, R. M., and Hahn, C. J.: A survey of changes in cloud cover and cloud types over land from surface observations, 1971–96, *J. Climate*, 20, 717, doi:10.1175/jcli4031.1, 2007.
- Weber, R. J., Sullivan, A. P., Peltier, R. E., Russell, A., Yan, B., Zheng, M., de Gouw, J., Warneke, C., Brock, C., Holloway, J. S., Atlas, E. L., and Edgerton, E.: A study of secondary organic aerosol formation in the anthropogenic-influenced southeastern United States, *J. Geophys. Res.-Atmos.*, 112, D13302, doi:10.1029/2007jd008408, 2007.
- Wilson, J. C., Lafleur, B. G., Hilbert, H., Seebaugh, W. R., Fox, J., Gesler, D. W., Brock, C. A., Huebert, B. J., and Mullen, J.: Function and performance of a low turbulence inlet for sampling supermicron particles from aircraft platforms, *Aerosol Sci. Tech.*, 38, 790, doi:10.1080/027868290500841, 2004.
- Wonaschuetz, A., Sorooshian, A., Ervens, B., Chuang, P. Y., Feingold, G., Murphy, S. M., de Gouw, J., Warneke, C., and Jonsson, H. H.: Aerosol and gas re-distribution by shallow cumulus clouds: An investigation using airborne measurements, *J. Geophys. Res.-Atmos.*, 117, D17202, doi:10.1029/2012jd018089, 2012.
- Zhang, X., Hecobian, A., Zheng, M., Frank, N. H., and Weber, R. J.: Biomass burning impact on PM<sub>2.5</sub> over the southeastern US during 2007: integrating chemically speciated FRM filter measurements, MODIS fire counts and PMF analysis, *Atmos. Chem. Phys.*, 10, 6839–6853, doi:10.5194/acp-10-6839-2010, 2010.